JUN 0 3 1988

Z 19 -A

C 13.46: 1315

NBS TECHNICAL NOTE 1315

COMPLETED

U.S. DEPARTMENT OF COMMERCE / National Bureau of Standards

Investigation of the Hydrogen Source for Masers

K.B. Persson
F.L. Walls

ORIGINAL

The National Bureau of Standards[1] was established by an act of Congress on March 3, 1901. The Bureau's overall goal is to strengthen and advance the nation's science and technology and facilitate their effective application for public benefit. To this end, the Bureau conducts research to assure international competitiveness and leadership of U.S. industry, science and technology. NBS work involves development and transfer of measurements, standards and related science and technology, in support of continually improving U.S. productivity, product quality and reliability, innovation and underlying science and engineering. The Bureau's technical work is performed by the National Measurement Laboratory, the National Engineering Laboratory, the Institute for Computer Sciences and Technology, and the Institute for Materials Science and Engineering.

The National Measurement Laboratory

Provides the national system of physical and chemical measurement; coordinates the system with measurement systems of other nations and furnishes essential services leading to accurate and uniform physical and chemical measurement throughout the Nation's scientific community, industry, and commerce; provides advisory and research services to other Government agencies; conducts physical and chemical research; develops, produces, and distributes Standard Reference Materials; provides calibration services; and manages the National Standard Reference Data System. The Leboratory consists of the following centers:

- Basic Standards[2]
- Radiation Research
- Chemical Physics
- Analytical Chemistry

The National Engineering Laboratory

Provides technology and technical services to the public and private sectors to address national needs and to solve national problems; conducts research in engineering and applied science in support of these efforts; builds and maintains competence in the necessary disciplines required to carry out this research and technical service; develops engineering data and measurement capabilities; provides engineering measurement traceability services; develops test methods and proposes engineering standards and code changes; develops and proposes new engineering practices; and develops and improves mechanisms to transfer results of its research to the ultimate user. The Laboratory consists of the following centers:

- Applied Mathematics
- Electronics and Electrical Engineering[2]
- Manufacturing Engineering
- Building Technology
- Fire Research
- Chemical Engineering[3]

The Institute for Computer Sciences and Technology

Conducts research and provides scientific and technical services to aid Federal agencies in the selection, acquisition, application, and use of computer technology to improve effectiveness and economy in Government operations in accordance with Public Law 89-306 (40 U.S.C. 759), relevant Executive Orders, and other directives; carries out this mission by managing the Federal Information Processing Standards Program, developing Federal ADP standards guidelines, and managing Federal participation in ADP voluntary standardization activities; provides scientific and technological advisory services and assistance to Federal agencies; and provides the technical foundation for computer-related policies of the Federal Government. The Institute consists of the following divisions:

- Information Systems Engineering
- Systems and Software Technology
- Computer Security
- Systems and Network Architecture
- Advanced Computer Systems

The Institute for Materials Science and Engineering

Conducts research and provides measurements, data, standards, reference materials, quantitative understanding and other technical information fundamental to the processing, structure, properties and performance of materials; addresses the scientific basis for new advanced materials technologies; plans research around cross-cutting scientific themes such as nondestructive evaluation and phase diagram development; oversees Bureau-wide technical programs in nuclear reactor radiation research and nondestructive evaluation; and broadly disseminates generic technical information resulting from its programs The Institute consists of the following Divisions:

- Ceramics
- Fracture and Deformation[3]
- Polymers
- Metallurgy
- Reactor Radiation

[1]Headquarters and Laboratories at Gaithersburg, MD, unless otherwise noted; mailing address Gaithersburg, MD 20899.
[2]Some divisions within the center are located at Boulder, CO 80303.
[3]Located at Boulder, CO, with some elements at Gaithersburg, MD

Investigation of the Hydrogen Source for Masers

K.B. Persson
F.L. Walls

Time and Frequency Division
Center for Basic Standards
National Measurement Laboratory
National Bureau of Standards
Boulder, Colorado 80303-3328

Supported by
Naval Research Laboratories
Washington, DC 20375

U.S. DEPARTMENT OF COMMERCE, C. William Verity, Secretary

NATIONAL BUREAU OF STANDARDS, Ernest Ambler, Director

Issued April 1988

National Bureau of Standards Technical Note 1315
Natl. Bur. Stand. (U.S.), Tech Note 1315, 56 pages (Apr. 1988)
CODEN:NBTNAE

U.S. GOVERNMENT PRINTING OFFICE
WASHINGTON: 1988

For sale by the Superintendent of Documents, U.S. Government Printing Office, Washington, DC 20402

CONTENTS

		Page
1.	Introduction	1
2.	Radio Frequency Discharge Characteristics	2
3.	Radio Frequency Discharge Circuit	5
4.	Dissociation of Molecular Hydrogen	6
5.	Surface Recombination	6
6.	Atomic Hydrogen Detector	11
7.	Measurements and Their Interpretation	16
8.	Lifetime Considerations	24
9.	Summary and Recommendations	27
10.	Acknowledgments	29
11.	List of Figures and Tables	30
12.	References	33

0
IV

INVESTIGATION OF THE HYDROGEN SOURCE FOR MASERS

K. B. Persson and F. L. Walls
Time and Frequency Division
National Bureau of Standards
Boulder, Colorado 80303

Various engineering and phenomenological aspects of the radio frequency discharge source for atomic hydrogen used in the masers have been investigated theoretically and experimentally to provide a base for minimizing the size of the source and its power consumption. A scheme and detector have been devised, permitting absolute detection of the atomic beam, and an atom-atom surface recombination theory was developed, applicable to the detector as well as to the walls of the discharge vessel. A self-starting radio frequency circuit, allowing as little as 0.1 W power consumption by the atom source, has been developed.

Key words: atomic hydrogen; atomic hydrogen detection; dissociation efficiency; hydrogen maser; radio frequency discharge; surface-recombination.

1. Introduction

Satellite operation of a hydrogen maser requires long life, small scale, and low power consumption. The objective of this investigation was to provide a basis for the design of a small, efficient hydrogen dissociator that runs on as little power as possible, and is self-starting. To reach this objective it was necessary to consider the dissociator radio frequency (rf) discharge, the manner of coupling of the rf power into it to achieve self-starting, volume production of the atomic hydrogen, loss of hydrogen atoms by surface recombination, and an absolute technique for measuring the atom flux emerging from the collimator of the dissociator [1]. For a general discussion of the plasma problem treated here see [1,2].

2. Radio Frequency Discharge Characteristics

Three different discharge bottles made of Pyrex, using three different rf electrode configurations as shown in figure 2.1, were used in the investigation. In all configurations shown, the rf power was coupled capacitively to the plasma inside the Pyrex bottles. None of the configurations are easily amenable to a theoretical description. Some understanding of the behavior of the discharge is obtained by considering the situation shown in figure 2.2, where the plasma is located between two plane parallel electrodes with the lateral dimensions large in comparison with the distance L between the electrodes, and with all dimensions represented by the area A of the electrodes small in comparison with the wavelength corresponding to the radio frequency.

Labeling the electric field just inside one of the electrodes with E_a and the field inside the plasma with E_p, we find, since the current density J is conserved, that

$$J = j\omega\epsilon_0 E_a = (j\omega\epsilon_o+\sigma_p)E_p \qquad (2.1)$$

where

$$\sigma_p = \frac{\epsilon_o\omega_p^2}{\nu+j\omega} \qquad (2.2)$$

is the complex conductivity of the plasma and

$$\omega_p^2 = \frac{e^2 n_e}{m\epsilon_o} \qquad (2.3)$$

the plasma frequency with n_e the electron density and m the electron mass, and with ν the momentum transfer frequency of the electrons colliding with atoms and molecules. As a result we find that

$$Z_p = \frac{L}{\epsilon_o A}\ \frac{\nu+j\omega}{(\omega_p^2-\omega^2+j\omega\nu)} \qquad (2.4)$$

and

$$\frac{E_p}{E_a} = \frac{1+\left(\frac{\nu}{\omega}\right)^2}{\left(\frac{\omega_p^2}{\omega^2}-1\right)^2+\left(\frac{\nu}{\omega}\right)^2} \qquad (2.5)$$

and

$$2\omega\epsilon_0 \frac{P}{|J|^2} = \frac{\frac{\nu}{\omega}\frac{\omega_p^2}{\omega^2}}{\left(\frac{\omega_p^2}{\omega^2}-1\right)^2+\left(\frac{\nu}{\omega}\right)^2} = \frac{2P}{\epsilon_0\omega|E_a|^2} \qquad (2.6)$$

where Z_p is the impedance between the rf electrodes, and P the power dissipated per unit volume. These three quantities, the plasma impedance Z_p, the electric field E_p inside the plasma, and the power P dissipated per unit volume, are strong functions of the electron density for low pressures (ν comparable to or less than the radio frequency $\omega \approx 10^9$ rad/s). The behavior of E_p and P as function of the electron density, in terms of the normalized quantity ω_p^2/ω^2, is shown in figure 2.3. The curves have well pronounced maxima in the neighborhood of plasma resonance ($\omega_p = \omega$).

The momentum transfer collision frequency in the formulas above is generally energy dependent. Lacking experimental information about collisions between hydrogen atoms and electrons, we use corresponding information derived from collisions between electrons and hydrogen molecules when a constant mean free path ℓ is an acceptable approximation. From electron mobility data [2] we find that

$$\ell p = 3.3 \times 10^{-2} \text{ Pa} \qquad (2.7)$$

where

$$\nu = \frac{c}{\ell} \qquad (2.8)$$

and

$$c = \sqrt{\frac{8kT_a}{\pi m}} \qquad (2.9)$$

is the mean thermal velocity for a Maxwellian energy distribution with the temperature T_e. The electron temperature is determined by the field E_p and can, in the constant mean free path approximation, be written as

$$T_e = \frac{\pi}{3}\frac{1}{k}\sqrt{\frac{M}{6m}}\,(eE_p\ell) \tag{2.10}$$

where k is Boltzmann's constant and M the mass of hydrogen atom or molecule. From the formulas above, we find that the collision frequency can be written as

$$\nu = \sqrt{\frac{8}{3}\sqrt{\frac{M}{6m}}\,\frac{eE_p}{m\ell}} \tag{2.11}$$

which shows the dependence on the plasma field E_p and mean free path ℓ.

The above formulas give a partial description of how the plasma responds to the applied rf field. To complete the description it is necessary to discuss how the plasma is generated by the rf field The power P, dissipated in the plasma, is primarily fed to the electron gas which in its turn loses power by elastic, exciting, and ionizing collisions. The exciting and ionizing collisions involve the high energy electrons in the tail of an essentially Maxwellian velocity distribution with the temperature T_e. The electrons and ions are lost to the walls of the discharge vessel by ambipolar diffusion with a diffusion coefficient essentially proportional to the electron temperature T_e. In the presence of the plasma resonance the electron density n_e is determined by the power density in a very nonuniform and nonlinear manner. The nonuniformities and nonlinear couplings are tempered by the fact that the electron temperature is very high (several electron volts), resulting in high heat conductivity in the electron gas. The poor thermal coupling between the electron gas and the walls leads to an almost uniform electron temperature, although the electron density still is nonuniform.

Most plasmas are nonuniform with the high electron density in the center of the plasma. At low power and correspondingly low electron density the plasma resonance starts in the center of the plasma. With increasing electron density the plasma resonance splits spatially in two parts with each part moving towards an rf electrode, creating regions with high power dissipation in front of each electrode. An important phenomenon associated with an rf discharge is the fact that it is self-limiting in terms of the power consumption and the electron density. This is due to the presence of the plasma resonance and is illustrated by eqs (2.5) and (2.6) as well as figure 2.3. Figure 2.3 shows that when the electron density or correspondingly ω_p^2/ω^2 increases beyond plasma resonance, the field E_p in the interior of the plasma decreases drastically relative to the applied field E_a with a subsequent decrease of power dissipated in the interior of the plasma. How and for what power this manifests itself depends on the location, configuration, and design of the rf electrodes, and the discharge vessel. Maximum electron density is obtained when $\omega_p^2/\omega^2 \simeq 1$, giving $n_e \simeq 2\ 10^8\ cm^{-3}$ at a frequency of 150 MHz.

3. Radio Frequency Discharge Circuit

The circuit used for running the discharge and measuring its power consumption is shown in figure 3.1. It consisted of a 150 MHz signal generator followed by a step attenuator, a power amplifier, a network permitting the measurement of reflected and transmitted power, and finally the network coupling the power to the discharge. In case A the output from the power amplifier was directly coupled to the electrodes which consisted of copper tapes glued, in opposite positions, to the cylindrical discharge vessel. The measurements done in this configuration proved very cumbersome. Every time the hydrogen flux was measured, the discharge had to be extinguished and reignited. In this configuration the discharge could be started only with the help of a Tesla coil even at the highest available rf power.

The discharge could be made self-igniting to as low power as 0.1 W. This was done by using a very low coupling to the autotransformer and tuning it with a trim capacitance to resonance in the absence of the discharge. When the discharge was lit it shorted the trim capacitance and presented an inductance in series with the discharge, as load to the power amplifier. The auto transformer required few turns which could be shaped and located close to or around the discharge bottle, occupying very little space. The only requirement was that the circuit had a high Q and good capacitive coupling to the discharge at the high voltage points.

4. Dissociation of Molecular Hydrogen

The dissociation by electron impact of molecular hydrogen and the various molecular states involved are summarized by Massey and Burhop [3] The cross section has been measured by Vroom and de Heer [4] and Mumma and Zipf [4]. The dissociation starts at about 8.8 eV with slowly increasing cross section, which reaches a maximum of about 10^{-17} cm^2 around 60 eV. The rate of production S of atoms per unit volume can be written as

$$S = 2n_e n_2 \overline{v_e Q_D} \qquad (4.1)$$

where n_e is the electron density, n_2 the molecular hydrogen density, and $\overline{v_e Q_D}$ the electron velocity times the dissociation cross section averaged over the normalized electron distribution function. The distribution function is particularly complicated for the case of the rf dissociators used in conjunction with the hydrogen masers. This is due to bottle and electrode configurations that are difficult to characterize in the presence of plasma resonance, and the low operating pressures which make collisions with the walls important. We therefore treat $\overline{v_e Q_D}$ as an empirical function.

5. Surface Recombination

The pressure of hydrogen in the dissociators is too low to consider volume recombination as a significant loss process for atomic hydrogen,

and it will be neglected. The only loss process for atomic hydrogen is then surface recombination. To describe this process we introduce the surface density n_s of atomic hydrogen, a capture cross section Q_s, and a sticking time T_s. The surface density n_s represents the number of hydrogen atoms per unit area sticking to the surface at any given time. The capture cross section is the area around an absorbed atom, within which an atom coming from the gas phase must impact in order to form a molecule. The steady state equation for conservation of atoms on the surface can be written as

$$n_1(R)c_1 = \frac{n_s}{T_s} + n_1(R)c_1 n_s Q_s \qquad (5.1)$$

where $n_1(R)$ is the atom density just inside the wall, and c_1 an appropriate thermal velocity average of the atoms hitting the wall. The left side is the flow density of atoms from the gas phase to the surface. The first term on the right side is the flow density of atoms leaving the surface after resting there the time T_s. The last term represents the loss of atoms on the surface due to formation of hydrogen molecules. The probability η, defined as $n_s Q_s$, that a hydrogen atom hits the surface and forms a molecule can, with the help of eq (5.1), be written as

$$\eta = n_s Q_s = \frac{1}{1 + \dfrac{1}{n_1(R)c_1 T_s Q_s}} . \qquad (5.2)$$

This formula shows not only that the probability η depends on T_s and Q_s, which are characteristic for the atom-surface interaction, but also that η depends on the density and temperature of the atom gas in front of the surface, and these are partially determined by the rf discharge.

To determine the atom density $n_1(R)$ in front of the surface or the beam collimating hole, we will use a simplified model of the rf discharge and the dissociation mechanism. We assume that the discharge bulb is spherical with the radius R. Using the source function S for generation of atoms, given by eq (4.1), but introducing a dissociation frequency ν_D defined as

$$\nu_D = n_e \overline{v_e Q_D} \tag{5.3}$$

where Q_D is the dissociation cross section, we can write the steady state equation for conservation of hydrogen atoms as

$$\frac{1}{r^2} \frac{\partial}{\partial r} (r^2 \Gamma_1) = \nu_D (n_o - n_1) \tag{5.4}$$

where Γ_1 is the atom flow density towards the walls, n_o the constant sum of the molecular and atomic hydrogen densities, and n_1 the atomic hydrogen density. The flow density Γ_1 is given by Fick's law

$$\Gamma_1 = -D_1 \frac{\partial n_1}{\partial r} \tag{5.5}$$

where D_1 is the diffusion coefficient for atomic hydrogen diffusing in molecular hydrogen. Eliminating the flow density between the two equations above, we find

$$\frac{1}{r^2} \frac{\partial}{\partial r} \left(r^2 \frac{\partial n_1}{\partial r} \right) - \frac{n_1}{\Lambda_1^2} = - \frac{n_o}{\Lambda_1^2} \tag{5.6}$$

where

$$\Lambda_1^2 = \frac{D_1}{\nu_D} . \tag{5.7}$$

Assuming that Λ_1 can be viewed as a constant we can write the solution to eq (5.6) as

$$n_1 = n_o - A_1 \frac{\sinh x}{x} , \quad x = \frac{r}{\Lambda_1} \tag{5.8}$$

where the integration constant A_1 is determined by the fact that the loss of atomic hydrogen on the surface must be balanced by the diffusive flow to the surface. This gives the equations

$$\eta n_1 c_1 = - \frac{D_1}{\Lambda_1} \frac{\partial n_1}{\partial x} , \quad x = \frac{R}{\Lambda_1} \tag{5.9}$$

and

$$A_1 = \frac{\eta n_0 c_1}{c_1 \eta f(x) + \frac{D_1}{\Lambda_1} \frac{\partial f(x)}{\partial x}}, \quad f(x) = \frac{\sinh x}{x}, \quad x = \frac{R}{\Lambda_1}. \qquad (5.10)$$

The spatial distribution of the atomic hydrogen and in particular the degree of dissociation $\alpha(R)$ in front of the collimator can now be written as

$$\alpha(R) = \frac{1}{1 + \frac{c_1 \eta \Lambda_1}{D_1} \left(\frac{\partial}{\partial x} \ell nf(x)\right)^{-1}}, \quad x = \frac{R}{\Lambda_1} \qquad (5.11)$$

Equations (5.2) and (5.11) show η and $\alpha(R)$ mutually depend on each other. Eliminating η between the two equations yields

$$\frac{1}{\alpha(R)} = \frac{(1-\gamma)}{2} + \sqrt{\left(\frac{1+\gamma}{2}\right)^2 + \gamma\vartheta} \qquad (5.12)$$

where

$$\gamma = n_0 c_1 T_s Q_s \qquad (5.13)$$

and

$$\vartheta = \frac{c_1 \Lambda_1}{D_1} \frac{I_0(R/\Lambda_1)}{I_1(r/\Lambda_1)} \left(\frac{\partial}{\partial x} \ell nf(x)\right)^{-1}, \quad x = \frac{R}{\Lambda_1}. \qquad (5.14)$$

The degree of dissociation $\alpha(R)$ given by eq (5.12) is obtained by assuming that the concentration of atomic hydrogen is sufficiently small so that the basic equations can be linearized. The result is also applicable when the relative molecular hydrogen density is small and diffuses in an almost stationary gas of atomic hydrogen. However, it is then necessary to replace c_1 and D_1, characteristic for atomic hydrogen, with c_2 and D_2, characteristic of molecular hydrogen.

The degree of dissociation, $\alpha(R)$, in front of the entrance to the collimator depends on two parameters γ and ϑ and is illustrated in figure 5.1 where it is shown as the fully drawn curves. The parameter γ

expresses the influence of the wall recombination on the product $T_s Q_s$. The variable ϑ accounts for the influence of the rf discharge through the dissociation frequency ν_D, defined by eq (5.3), and approximately inversely proportional to the rf power. The degree of dissociation is bounded by two limiting forms represented by the broken curves. The high limit, $\alpha(R) = 1$, is obtained when the wall recombination is negligible and generated by letting γ approach zero. This limit is independent of the rf power. The lower limit is obtained when any atom hitting the wall is lost immediately by forming a molecule. It is generated by letting γ approach infinity. This limit is a function of the rf power. High degree of dissociation is obtained at small rf powers provided the wall recombination is small, but it is also obtained when wall recombination is high provided we use high rf power.

The relation between the variable ϑ and the dissociation frequency ν_D is better illuminated by using approximate forms of ν_D. It can be shown that

$$\vartheta \sim \frac{2c_2}{k\nu_D} \quad \text{for} \quad \nu_D < \frac{4D_2}{R^2} \tag{5.15}$$

and

$$\vartheta \sim \frac{c_2}{\sqrt{D_2 \nu_2}} \quad \text{for } \nu_D > \frac{4D_2}{R^2} \, . \tag{5.16}$$

The dissociation frequency ν_D is a very complex function of the properties of the rf discharge but generally increases with increasing rf power. The dissociation frequency ν_D is approximately proportional to the power dissipated per particle in the dissociator, atom or molecule, and can be written as

$$\nu_D \propto \frac{P}{R^3 n_0} \tag{5.17}$$

where P is the total rf power, n_0 the particle density, and R the radius of the spherical container. In the low power limit, corresponding to the approximation given by eq (5.15), we can write eq (5.12) as

$$\frac{1}{\alpha(R)} = \frac{1-\gamma}{2} + \sqrt{\left(\frac{1+\gamma}{2}\right)^2 + \gamma K \frac{R^2 p}{PT^{\frac{1}{2}}}} \qquad (5.18)$$

where K can be viewed as a constant. From this formula we draw the conclusion that the degree of dissociation $\alpha(R)$ increases with increasing power and temperature, while it decreases with increasing pressure and radius of the dissociator. For operating the dissociator at small powers, γ or the wall recombination must be very small.

6. Atomic Hydrogen Detector

The design of an absolute detector of the hydrogen atomic flux S that leaves the exit hole of the collimator is in principle identical with that of a bolometer used for detection of infrared radiation. A resistive, temperature-sensitive element, with a surface that encourages atom recombination, intercepts the atom flux. With a properly prepared surface all the atoms recombine on the surface, release the recombination energy, and heat the temperature sensitive element. The relative change of the resistance is proportional to the atom flux.

The atomic flux detector is best described by using the same theory that used in the discussion of surface recombination in section 5. The introduction of a sticking time T_s, a capture cross section Q_s, and conservation of atoms on the surface of the detecting element then leads to the following expression for η, the probability of surface recombination

$$\eta = n_s Q_s = \frac{\beta S Q_s}{\left(\frac{4\pi r^2}{T_s} + \beta S Q_s\right)} \qquad (6.1)$$

where β is the solid angle of the atom flux, and r the distance between the detecting element and the exit hole of the collimator, viewed as a point source. The power P_1 released to the detecting element then becomes

$$P_1 = eSE_D\eta = \frac{\beta S^2 Q_s E_D e}{\left(\frac{4\pi r^2}{T_s} + \beta S Q_s\right)} \qquad (6.2)$$

where E_D is the recombination energy in electron volts. The highest sensitivity and the largest range of proportionality between P_1 and S are obtained when r is as small as possible and the sticking time T_s is as large as possible. We have

$$P_1 = SE_D e \qquad (6.3)$$

provided that

$$S \gg \frac{4\pi r^2}{\beta T_s Q_s} \qquad (6.4)$$

Traditionally the atomic hydrogen detector is made of platinum because of its high and reliable temperature coefficient of resistivity, and because it is a good catalyzer for the recombination process; that is, the sticking time T_s for platinum is long. The platinum detector element is usually made in the shape of a very fine wire or strip with a resistance in the range 50 to 150 Ω, creating mechanical difficulties in its handling, and giving a very small beam intercepting cross section. These difficulties were eliminated by providing the mechanical strength by a thin, high temperature polyimide film (25 μm thick) on which platinum was evaporated in layers 15 to 20 nm thick. The dimensions of the strips are shown in figure 6.1. The ends of the strips were reinforced with additional evaporated platinum to provide good electrical and thermal contacts to the strip holders. The strips were clamped to heavy metal supports with high thermal mass, controlling the end temperatures of the strip, and incorporated in the bridge illustrated in figure 6.2, with the platinum facing the exit hole of the collimator. The resistances of the bridge elements were chosen approximately equal, with R_o, the resistance of the platinum element at the temperature T_o (room temperature) of the supports, in the range 70 to 130 Ω. The resistance R_1 was chosen slightly larger than R_o and the bridge balanced by adjusting the bridge voltage V_o until the resistance of the platinum element, due to ohmic heating, was equal to R_1. The

additional heating of the platinum element due to recombination of the atoms on its surface gave rise to an unbalanced voltage ΔV proportional to the atomic flux S. The photons generated in the discharge that reach the platinum element from the collimator should also be included in the power balance of the bridge. However a crude evaluation of their influence indicates that their contribution is negligible in so far as this investigation is concerned.

Two calculations must be done in order to obtain the proportionality constant C between the atomic flux S and the unbalanced voltage ΔV of the bridge. The first accounts for the relative change $\Delta R/R_0$ in the resistance of the platinum element when the bridge first was balanced. The second calculation accounts for the temperature distribution and the resulting $\Delta R/R_1$ caused by the atomic hydrogen flux hitting the center of the platinum element. Both calculations are based on the same differential equation

$$\frac{\partial^2 T}{\partial x^2} - \frac{T-T_a}{A^2} = -\frac{P}{\sigma} \qquad (6.5)$$

where P is the dissipated power per unit volume while the boundary conditions are

$$T = T_0 \text{ for } x = \pm \ell \qquad (6.6)$$

with ℓ the length of the platinum strip with $x = 0$ in the center, and with the characteristic length A defined by

$$A^2 = \frac{\delta\sigma}{2\gamma} \qquad (6.7)$$

where δ is the thickness of the platinum strip, σ its heat conductivity and γ the proper coefficient for the linearized radiation law. The linearization of the radiation law is justified by the fact that the platinum element is only slightly warmer than the environment. The first term in eq (6.5) represents the heat conduction, the second term the heat

loss, and the third term the power dissipated per unit volume in the platinum element either by ohmic heating or by recombination of the hydrogen atoms.

In the case of ohmic heating of the platinum element we assume that the power is dissipated uniformly and therefore

$$P = \frac{P_o}{2\delta d\ell} \tag{6.8}$$

where P_o is the total dissipated power, and d the width of the platinum strip. We then obtain the temperature distribution

$$T-T_o = \frac{P_o \Lambda^2}{2\ell\delta d\sigma}\left(1- \frac{\cosh x/\Lambda}{\cosh \ell/\Lambda}\right) \tag{6.9}$$

and a relative change in the platinum resistance of

$$\frac{\Delta R}{R} = \frac{\alpha P_o}{2\gamma d\ell}\left(1 - \frac{\Lambda}{\ell}\frac{\sinh \ell/\Lambda}{\cosh \ell/\Lambda}\right) \tag{6.10}$$

where α is the temperature coefficient of the platinum resistance. In the limit $\Lambda \ll \ell$, justified by the design parameters, the relative resistance change can be written as

$$\frac{\Delta R}{R} = \frac{R_1 - R_o}{R_o} = \frac{\alpha P_o}{2\gamma d\ell} \tag{6.11}$$

with the second equality obtained when the bridge is first balanced, and the power P_o written as

$$P_o = R_1\left(\frac{V_o}{R_1+R_2}\right)^2. \tag{6.12}$$

Turning on the hydrogen beam dissipates a power P_1 given by eq (6.3) in the center of the platinum strip. The linearity of the original differential equation allows us to solve for the resulting temperature distribution, independent of the ohmic heating created when the bridge was first balanced. Treating the power source due to recombination of the atoms as a delta

function in the center of the platinum element, we find the temperature distribution

$$T-T_o = \frac{\Lambda P_1}{4\delta\sigma d} \frac{\sinh\left(\frac{\ell}{2\Lambda} \pm \frac{x}{\ell}\right)}{\sinh\frac{\ell}{2\Lambda}} \qquad (6.13)$$

where the different signs apply to the different sides of the positive delta function. This temperature distribution gives rise to a relative resistance change which in the limit $\Lambda \ll \ell$ can be written as

$$\frac{\Delta R}{R_1} = \frac{\alpha P_1}{4\gamma d\ell} \qquad (6.14)$$

Eliminating the group of parameters

$$\frac{\alpha}{\gamma d\ell}$$

between eqs (6.11) and (6.14), P_o with the help of eq (6.12), and P_1 with the help of eq (6.3) as well as converting the relative resistance change due to the recombination power into a voltage response ΔV of the bridge, one finds that

$$\Delta V = CS \qquad (6.15)$$

where

$$C = \frac{(R_1+R_2)(R_1-R_n)}{2R_oV_o} eE_D \qquad (6.16)$$

The consequence of this result is that detailed knowledge of the platinum element is not needed. The necessary proportionality constant is obtained from the bridge parameters and the voltage V_o required to balance the bridge in the absence of the atom flux, provided the design of the platinum element conforms to the basic assumptions used in the derivation. The first requirement is that the cross-sectional area of the beam is centered on, and small in comparison with, the area of the platinum strip. The second

requirement is that the characteristic length Λ is significantly smaller than the length ℓ of the platinum element. Typical design parameters we used were

	Platinum	Polyimide
d(cm)	0.6	0.6
δ(cm)	2×10^{-6}	2.5×10^{-3}
ℓ(cm)	2	2
$\sigma(W(cmK)^{-1})$	0.71	1.9×10^{-4}
$\gamma(W(cm^2K)^{-1})$	$\sim8\times10^{-5}$	$\sim8\times10^{-5}$
Λ(cm)	2	2
$2\Lambda/\ell$	9×10^{-3}	5.5×10^{-2}
$E_D e(J)$	3.5×10^{-19}	

Typical values for the bridge parameters and resulting proportionality constant were

V_o	5.19 V
R_o	61.7 Ω
R_1	70 Ω
R_2	100 Ω
C	7.74x10-19 V s^{-1}

In a representative set of measurements we used a 4 mm long collimating hole with a diameter of 0.4 mm. The pressure in the dissociator was 4.7 Pa with 1.3×10^{-6} Pa (10^{-6} T) in the pump chamber and with the platinum strip located about 5 mm from the exit hole of the collimator. At a rf power of 4 W we obtained a bridge unbalance of 2 mV corresponding to a recombination power of 0.91 mW. Assuming that all hydrogen atoms recombined on the platinum surface, this corresponds to an atom flux of 2.6×10^{15} s^{-1}.

7. Measurements and Their Interpretation

The principal measurements were the atomic hydrogen flux emerging from the exit of the collimator as function of the rf power P, the

dissociator pressure p, the dissociator wall temperature T, and the intensity of the atomic H_α spectral line. The state of the dissociator, in terms of impurities, was determined with the help of a high quality hand spectrometer. No measurements were taken unless only the three lines H_α, H_β, and H_γ were observed. In addition, the degree of dissociation was obtained from the pressure changes generated when the discharge was turned on and off. Measurements were done on the three types of bottles shown in figure 2.1.

Considerable difficulties in terms of drift and instabilities were experienced in the early use of the platinum element. Part of the difficulties were traced to unreliable electrical contacts to the ends of the platinum element. These difficulties were eliminated by coating the contact surfaces of the strip holder with indium. The remaining part of the drift seemed to be associated with slow initial changes in the resistance of the platinum element and was cured by running it for a few days at a slightly elevated temperature.

All dissociator bottles were made of Pyrex, and the spectrum from most of them indicated the presence of molecular hydrogen and impurities. The degree of dissociation increased and the impurities disappeared from the spectrum after the dissociator had been run from several hours to many days, depending on an unknown correlation with the past history of the bottles. All bottles eventually cleaned up and exhibited the pure line spectrum of atomic hydrogen and a purplish-red discharge color. Immediately after the discharge was turned on, the spectrum of two of the dissociator bottles was that of pure atomic hydrogen. However, the spectrum deteriorated very rapidly and returned to a pure atomic spectrum only after a rather substantial time. This observation indicates that the impurities did not come directly from the gas phase but rather from the walls of the dissociator, where they were stored either as absorbed surface layers or inside the glass matrix. These impurities were released by bombardment of the walls by electrons, ions, and photons generated by the discharge, and removed from bottle by the hydrogen flow. A conclusion from the observations above was that clean Pyrex, in equilibrium with atomic or molecular hydrogen gas, has a surface with low

probability for recombination of atomic hydrogen. Based on this reasoning we decided to process the dissociator bottles in the following manner. The bottle was made with an inlet and outlet much larger than the collimating hole and placed in an oven in such a manner that clean hydrogen flowed through the bottle at the annealing temperature of Pyrex, 550°C. After the bottle was annealed for about eight hours, it was attached to the vacuum system as soon as possible. This processing allowed the impurities to diffuse out of the glass matrix and be replaced by hydrogen at as high a temperature as possible. Bottles processed in this manner showed about a factor of 4 decreas in the time required to reach the state of cleanliness necessary for the measurements.

The first set of measurements was done on bottle A, figure 2.1, the largest bottle. The rf electrodes consisted of two copper foils 1.5 cm x 3 cm glued to opposite sides of the bottle and coupled directly to the output of the rf amplifier, scheme A of figure 3.1. The discharge was not self-igniting within the available power range, causing considerable difficulties and scattering in the measurements. A measurement consisted of observing the change in ΔV of the bridge, obtained by turning the rf discharge on, waiting three to four times the thermal time constant of the platinum element (4 to 5 sonds), and then turning the discharge off. In every measurement it was necessary to start the discharge with a Tesla coil, which upset the dc instruments attached to the bridge. The measurements that could be done are shown in figure 7.1. These measurements are also displayed in figure 5.1 where they have been displaced to conform as well as possible in slope and curvature with the theoretical curves. The displacements are somewhat arbitrary. The agreement with the theoretical curves cannot be considered evidence for the correctness of the theory although it lends it plausibility. There are many possibilities for error in the plotted variables. The discussion in section 6 of the atomic hydrogen detector indicates several possibilities for errors which are all expressed in eq (6.4). The present lack of knowledge of the T_s and Q_s makes it impossible to make a theoretical evaluation of the errors, and our experimental apparatus was too crude to obtain them experimentally to better than a factor of two.

It is possible to make some evaluation of the measurements by comparing the atom flux Γ_1, measured by the platinum element, and the total flux Γ_o going through the collimator. The total flux was obtained either by measuring the pump current as a function of the dissociator pressure, or by measuring the dissociator pressure as a function of time, after the source of hydrogen was shut off. A simple derivation, based on long mean free path and geometrical considerations of the collimator gives

$$\Gamma_1 = \pi a^2 \frac{\bar{nv}}{4} \frac{1}{\left[1 + \left(\frac{\ell}{2a}\right)^2\right]} \quad \ell > a \quad \bar{nv}\pi \frac{a^4}{\ell^2} \tag{7.1}$$

where a is the radius and ℓ the length of the collimator hole, n the density and

$$\bar{v} = \sqrt{\frac{8kT}{\pi M}} \tag{7.2}$$

the average thermal velocity of the gas in the dissociator, and where the last factor in eq. 7.1 is due to the geometry of the collimator. Similarly we find that

$$\Gamma_o = \frac{\bar{nv}}{4} \pi a^2 \frac{1}{2\left(1 + \frac{\ell}{a}\right)} \quad \ell > a \quad \frac{\bar{nv}}{8} \pi \frac{a^3}{\ell} \tag{7.3}$$

with the last factor representing the probability that an atom, making randomizing collisions with the inside wall of the collimator, leaves through the exit hole of the collimator. The aspect ratio $2a/\ell$ is generally so small that the approximate forms of the equations are applicable, giving the flux ratio of

$$\frac{\Gamma_1}{\Gamma_o} = \frac{8a}{\ell} \tag{7.4}$$

assuming 100% dissociation within the bulb and that every collision with the collimator results in recombination.

The errors in the derivation of the formulas for the fluxes are of the same nature and likely to be eliminated in the ratio. This ratio is used as a number of merit in the comparison and evaluation of the different dissociators. With an aspect ratio 1/10 the theoretical flux ratio becomes 0.4. This large ratio and the small solid angle of the collimated beam give a high relative flux density within the collimator beam. When the platinum element was taken out for inspection, it showed a very distinct image in the platinum coating corresponding to the expected cross section of the atom beam.

The dissociators were compared at 1 W rf power dissipated in the discharge. Table 7.1 shows the pertinent data for bottle A with a collimator hole radius of 0.2 mm and the aspect ratio of 1/10. The flux ratio is a factor of 3 to 4 less than expected from theory. This could be caused by a variety of factors, the most likely associated with the odd shape of the glass bottle, with the collimator located in a small diameter appendage.

The pressure dependence of the atom flux from bottle A is shown in figure 7.2. It indicates a qualitative agreement with the theory illustrated in figure 5.1. For a given γ and decreasing pressures the degree of dissociation approaches unity asymptotically. The atom flux becomes almost proportional to the pressure. With increasing pressure the degree of dissociation decreases and the atom flux starts to level off. The dissociator becomes less efficient at higher pressures. Physically this depends on the fact that at higher atom densities, larger fractions of the interior dissociator surfaces are covered by atomic hydrogen, resulting in higher surface recombination rates at higher pressures than at lower pressures.

Measurements showing the effect of the temperature of dissociator A on the atom flux are shown in figure 7.3. These measurements were done after the interior surfaces of the dissociator had been exposed to air. The measurements were made at a rf power level of about 6 W in the order A, B, C, and D and started immediately after the spectroscope showed

a clean atomic hydrogen line spectrum. In the first set of measurements A, the atom flux showed a rather strong decrease with increasing temperature, more than expected from a theoretical consideration. The simple theory predicts that the atom flux is proportional to the density of the atoms and their average thermal velocity, that is, the relative change in the atom flux due to a temperature change should be written as

$$\frac{\Delta\Gamma}{\Gamma} \leq \frac{1}{2}\frac{\Delta T}{T} \qquad (7.5)$$

The atom density change due to a temperature change at constant pressure is less than predicted by simple kinetic theory due to the influence of the wall recombination on the density change, as reflected in the pressure dependence shown in figure 7.2. Atom in flux measurements of bottles A initially violates eq (7.5). The dissociator was then run for 72 hours before the B, C, and D sets of measurements were made (figure 7.3). The results from these measurements do satisfy equation 7.5. This experience showed that an apparently clean dissociator could still have impurities on the walls detrimental to the production of hydrogen atoms, and that a proper processing of the bottles is essential.

The measurements on the medium size Bottle B, illustrated in figure 2.1, are displayed in figures 7.4 to 7.8. For these measurements the tuned autotransformer arrangement discussed in section 3 was used, allowing for self-ignition of the discharge at very low powers. The measured atom flux as function of the rf power (fig. 7.4), the pressure (fig. 7.6) and the temperature (fig. 7.7) behave essentially in the same way as the data obtained with the large bottle A. Two collimator sizes were used, the large one with a diameter of 0.4 mm and the small with a diameter of 0.1 mm, both with the aspect ratio of 1/10. The data obtained at 1 W with the large collimator are shown in table 7.2 while the small collimator data are shown in table 7.3.

Measurements of the flux ratio Γ_1/Γ_o suggest that the small dissociator was more efficient than the large and that the small collimator was more efficient than the large collimator. That the largest dissociator was

least efficient is most likely explained by the fact that the collimator was farthest away from the center of the discharge and that the discharge did not completely fill the dissociator. This would result in lower atom density in front of the collimator and a smaller atomic flux Γ_1, while the total flux Γ_o would remain unchanged, resulting in a smaller flux ratio for the larger bottles than for the smaller bottles. The fact that the large collimator was less efficient than the small collimator has to do with mean free path considerations. Based on kinetic theory and cross sections one finds, at the pressure of 6.7 Pa that the mean free path for the H_2-H_2 collisions is about 2 mm while it is about 1 mm for the H-H collisions. Both these mean free paths are comparable with the dimensions of the large collimator, in particular for the H-H collisions. The effect of a mean free path comparable with the collimator dimensions is to decrease the fluxes relative to the fluxes predicted by the collision free theory as well as to increase the collimation angle for the species with the smallest mean free path. As a result the large collimator will appear less efficient than the collimator which is small in comparison with the mean free path.

When the spectroscope showed a pure atomic hydrogen line spectrum it was assumed that the hydrogen was close to fully dissociated. This is a subjective judgement, verifiable only through very involved and cumbersome spectroscopic measurements of the molecular hydrogen concentration, a task beyond the scope of this investigation. Our conclusion from the spectroscopic observation was to some degree verified by observing the relative pressure changes obtained as a function of the power when the discharge was turned on and off. We can view the dissociator as two, well communicating volumes V_o and V_1 connected to the rest of the system through two very small leaks, the inlet leak valve and the outlet collimator.

The volume V_o is the volume of the dissociator, and V_1 the volume created by the leak valve and the glass tubes connecting it to the dissociator. If the inlet and outlet leaks are sufficiently small, we can view the system as closed during a measurement. Simple theoretical considerations assuming T constant then give

$$\frac{p_1 - p_o}{po} = \frac{\alpha V_o}{2V_1 + (2-\alpha)V_o} \qquad (7.6)$$

where p_o and p_1 are the pressures before and after the discharge has been turned on, respectively. A set of measurements of the pressure changes as function of the rf power is shown in figure 7.8, where the discharge was turned on and off with a cycle of 44 s., a time short relative to the time constant (several minutes) for the pressure changes due to the inlet and outlet leaks. On the left-hand side of this figure is the scale for the degree of dissociation α, where it has been assumed that the two volumes V_o and V_1 are equal. The data obtained at the highest pressure, 11 Pa has very little scatter and imply that the degree of dissociation was unity for rf powers above 0.4 W. The data obtained at the lower pressures show more scattering with an average degree of dissociation of about 0.8, lower than anticipated from the spectroscopic observations and the measurements of the atom flux. This discrepancy is most likely associated with a nonlinear pressure scale (thermocouple pressure gauge). These measurements show that with a proper instrumentation and development of theory, which takes into account the effects of the hydrogen flow through the system, the pressure measurements could be developed into a good tool for measurement of the degree of dissociation.

The third dissociator, bottle C of figure 2.1, was designed to test not only a still smaller bottle, but also to illuminate, and possibly suppress the influence of the plasma resonance. A long, small diameter bottle with the rf electrodes at the ends decreases the polarization of the plasma due to the plasma resonance. Plasma resonance is still present but occurs at a higher electron density. The first set of measurements, shown in figure 7.9, illustrates how the rf power P necessary to maintain the plasma varies with the intensity I of the H_α spectral line. Measurements at three different pressures are shown, all with pronounced maxima, which shift to higher intensities I with increasing pressure. The curves bear a striking resemblance to the broken curves in figure 2.3

which represent the theory for an idealized configuration around plasma resonance, and where the normalized rf power is plotted as function of the normalized electron density. The resemblance between the two sets of curves is not surprising, considering that the intensity of the H_α line is proportional to the electron density. The theory for the dissociator bottle C and the associated rf electrodes is too complex to include in this report. Suffice it to say that the presence of the plasma resonance mechanism generally gives rise to an upper limit for the power dissipated in the plasma, and that for some configurations this will give rise to two modes operating at the same power but on opposite sides of the maximum.

The measurements of the atom flux from dissociator bottle C, shown in figure 7.10, also reflect the presence of plasma resonance. The curves show well developed maxima versus rf power, with the maximum power decreasing with increasing pressure. The resulting two branches behave differently. In the lower branch, corresponding to low electron density and low electron temperature, the atom flux increases with increasing power. In the upper branch, corresponding to higher electron density and temperature, there is a slight tendency for the atom flux to increase with decreasing power. The fact that the upper branch is almost independent of the power, implies nearly full dissociation of the hydrogen. The data obtained at 1 W rf power are shown in table 7.4. The average, 0.41, of the flux ratios is close to the value 0.40 as predicted by the simple theory represented by eq (7.3) for fully dissociated hydrogen.

Of the three bottle sizes we tested it appears that the smaller the bottle is, the higher is the dissociation efficiency. The smallest bottle appears close to the theoretical limit, in general agreement with the theory proposed in section 5.

8. Lifetime Considerations

None of the bottles tested showed any deterioration after they had been processed until a clean atomic hydrogen line spectrum was observed. The traditional signs of deterioration like "white out" and "brown out" were not

observed. We attribute this to the fact that we used a very clean vacuum system, well processed dissociators, and an uncontaminated source of hydrogen as well as low power. We have no solid experimental evidence on which to base an estimate of the dissociator lifetime, but will nevertheless advance some points of view we think are important.

In most cases the dissociator had to be run a few days before it was clean, as judged by the spectrum and the atomic flux. In some cases the dissociator appeared very clean the moment it was first started, but deteriorated in a few minutes to a whitish discharge, characteristic for dirty hydrogen. Running it from a few hours to days restored it to its original condition with a reddish-purple discharge color, characteristic of clean atomic hydrogen.

The impurities that appear in the hydrogen dissociator, assuming that the hydrogen source is clean, have three different origins: the interior glass surface, the interstitial voids in the glass, and the glass matrix itself.

The impurities adsorbed on the interior glass surface are weakly bound and easily detached by bombardment of the wall by ions for the discharge. These impurities are most likely responsible for the very rapid deterioration of the discharge, when an originally very clean dissociator is first started. They represent a finite source and are eventually carried away with the hydrogen flow through the collimator.

The interstitial voids in the glass are filled with gases originating in the glass manufacturing process (ovens and flames). The rate of removal of these impurities is limited by the slow process of diffusion through the glass matrix. These impurities should be viewed as a finite but large source. The rate of their removal increases with increasing temperature and can cause long term deterioration of the dissociator if it is run at high temperature. The rate of diffusion into the bottle may then be larger than the rate of removal through the collimator, causing a steady increase of the impurity density in the

dissociator. This problem can be solved by running the dissociator at low temperature, decreasing the rate of diffusion, or by removing the impurities from the glass before the dissociator is attached to the maser. The removal of these types of impurities is traditionally realized by baking the glass bottle under vacuum at temperatures in the range 400 to 450°C (Pyrex). In the case of the hydrogen dissociator, where hydrogen is not an impurity, one can obtain a better result by letting clean hydrogen, at atmospheric pressure, flow through the bottle during the baking, which now can be done at higher temperatures than during the vacuum processing.

The third source of impurities is the glass matrix itself. It may be broken down into gaseous components due to bombardment by energetic particles from the plasma. This source must be viewed as infinite and can be tolerated only if the rate of production of the impurities is less than the rate of removal through the collimator. It is a likely cause of a finite life of the dissociator and related to the design of the rf electrodes. Except for the areas just under the rf electrodes, the bombardment of walls by the electrons and ions is governed by ambipolar diffusion and a wall sheath where the ions may acquire an energy of the order 10 eV. Both the rate of production of ions and electrons per unit volume and the power dissipated per unit volume in a fully developed, ideal rf plasma (at the maximum of the dissipated power) are proportional to the electron density or the square of the applied frequency. Both the total dissipated power and the total ion flux hitting the walls are then proportional to the volume of the dissociator. The ion flux density hitting the walls of spherical bottle is therefore proportional to the radius of that bottle and that the destruction of the walls decreases with decreasing radius. A smaller bottle then means longer life. However, the smaller the dissociator is, the higher is the electric field necessary for starting the discharge. The requirements that the dissociator is self-starting and has a long life are therefore conflicting requirements, making it necessary to design the circuit so that, in the absence of the discharge, the electric field inside the bottle is as high as possible for any given input power as was done in the circuit B shown in figure 3.1

The situation is considerably more complex in the area underneath the rf electrodes. This is the region where the rf fields, and the dc sheath fields are highest. The high sheath fields are caused partly by high electron temperature and partly by rectification of the rf fields, both enhanced by the resonance mechanism. According to other investigators, the first evidence of white-out shows up in this region. The influence of this source of impurities can be decreased by any means that decrease the effects of plasma resonance. The small bottle C shown in figure 2.1 represents such an attempt. It is made long with a small diameter to enhance the resistive part of its impedance relative to the capacitive part. It has ring electrodes, simulating Faraday cages, to reduce the ion bombardment of the walls underneath the electrodes. The overall effect of this configuration is to suppress the polarization of the plasma and achieve higher electron densities than predicted by the ideal plasma resonance. The data obtained with the small bottle C show a definite influence of the configuration and is possibly the most efficient bottle we have tested.

9. Summary and Recommendations

A theory for surface recombination of atomic hydrogen has been developed which is applicable both to the interior surfaces of the dissociator, where the aim is to suppress recombination, and to the surface of the atomic hydrogen beam detector, where the desire is to enhance recombination. The theory is based on the introduction of a surface sticking time T_s and a surface capture cross section Q_s, permitting a theoretical connection between the probability for recombination on the surface to the degree of dissociation of the gas just inside the surface. The theory agrees qualitatively with the experimental data. Better agreement is not expected due to lack of information about T_s and Q_s.

The atomic hydrogen beam detector was designed by vaporizing a thin layer of platinum on a film of high temperature plastic, permitting large enough detector area to completely intercept the collimated atom beam. A theory developed to apply to this composite element shows that, in spite of its complex nature, a measurement of the atom flux can in principle be viewed as

absolute. Unfortunately, the apparatus using this platinum element was not flexible enough to determine that all atoms in the collimated beam lead to recombination on the platinum element. The measurements must be viewed as minimum measurements.

The atom flux from three different sizes and configurations of dissociator bottles and rf electrode configurations was measured as function of the rf power dissipated in the plasma, the pressure, and the bottle's temperature. An attempt to measure the degree of dissociation by the pressure changes in the dissociator bottle, caused by turning the discharge on and off, was also made. With some reservations, caused by the uncertainty in the location of the platinum element, the atom flux measurements versus the rf power indicated that the smallest dissociator bottle was most efficient in producing atomic hydrogen, a result supported by the pressure changes obtained when the discharge was turned on and off. The spectroscopic observations implied that the gas in the larger bottles with larger collimators also was fully dissociated, a fact not confirmed by the measurements of the flux ratios. This discrepancy may be explained by the fact the discharge was not filling the larger dissociator bottles, leading to lower atom densities in front of the collimator entrance, and by the fact that the mean free path in atomic hydrogen was comparable with the dimensions of the larger collimator. Measurement of the atom flux versus the bottle temperature showed that the flux changes were due to the density changes caused by the temperature as well as the change in average thermal velocity in the change from molecules to atoms due to the dissociation process. Larger changes could be associated with release of impurities from the walls due to the temperature increase.

The theory for surface recombination, the measurements of the atom flux, the discussion of various mechanisms that influence the life of the dissociator, all indicate that a small dissociator bottle, operated at low powers, is likely to be more efficient and have longer life than a large bottle. The choice of size of bottle is however also influenced by the constraint that the discharge must be self-starting. In general, the smaller the bottle, the higher the rf field required for self-starting. This self-starting constraint was not evident for any of the bottles, provided a

tuned autotransformer was used as coupling element between the rf power sources and the discharge. This implies that still smaller bottles could be used.

The uncertainty in the conclusions based on the results from this investigation depends to high degree on the fact that the only experimental apparatus used in this investigation was put together before the pertinent theories and understanding were developed. With the present knowledge and a redesign of the experimental apparatus, better data could be obtained. The major uncertainty in the experimental set-up was due to the difficulties in orienting the platinum element so that the collimated atom beam hits its center. Any future design should provide a possibility to vary the distance between the platinum element and the exit hole of the collimator. One can then measure the product $T_s Q_s$ and determine the efficiency of the platinum element with regard to recombination, and obtain a better determination of the useful atom flux. A future investigation should also develop the pressure measurement method into a more precise method for measuring the degree of dissociation inside the dissociator bottle so that the recombination loss of atoms in the collimator can be evaluated. All bottles and collimators used in this investigation were made of Pyrex. A general conclusion was that the sticking time of hydrogen on a well cleaned Pyrex surface is short, leading to a small probability for surface recombination. This does not exclude the possibility that the use of other materials could lead to a better dissociator both from the atom yield point of view and life. This investigation has also demonstrated that plasma resonance mechanism, acting through the bottle and rf electrode configurations, has an influence on the atom yield of the dissociator, a point that should be considered in future work.

10. Acknowledgments

The authors gratefully acknowledge the support of the Naval Research Laboratories for this work.

11. List of Figures and Tables

Figure		Page
2.1	The dissociator bottles.	34
2.2	The plane-parallel case.	35
2.3	The plasma resonance.	36
3.1	The rf circuit.	37
5.1	The degree of dissociation.	38
6.1	The platinum element.	39
6.2	The bridge circuit.	40
7.1	Atom flux versus power. Bottle A.	41
7.2	Atom flux versus pressure. Bottle B.	42
7.3	Atom flux versus temperature. Bottle A.	43
7.4	Atom flux versus power. Bottle B.	44
7.5	Atom flux versus power. Bottle B.	45
7.6	Atom flux versus pressure. Bottle B.	46
7.7	Atom flux versus temperature. Bottle B.	47
7.8	Pressure change versus power. Bottle B.	48
7.9	Power versus H_α intensity. Bottle C.	49
7.10	Atom flux and plasma resonance.	50

Table

7.1	Dissociation efficiency of bottle A	31
7.2	Dissociation efficiency of bottle B	31
7.3	Dissociation efficiency of bottle B	32
7.4	Dissociation efficiency of bottle C	32

Table 7.1 Dissociation efficiency of bottle A

Discharge power is 1 W, collimator is 0.2 mm radius by 4 mm long.
Γ_0 is the estimated total flux, and Γ_1 is the atomic flux.

Discharge pressure	Γ_0	Γ_1	Γ_1/Γ_0
Pa	s^{-1}	s^{-1}	
8.0	1.04×10^{16}	7.8×10^{14}	0.075
5.0	6.86×10^{15}	5.4×10^{14}	0.079

Table 7.2 Dissociation efficiency of bottle B

Discharge power is 1 W, collimator is 0.2 mm radius and ℓ = 4 mm long,
Γ_0 is the estimated total flux, and Γ_1 is the atomic flux.

Discharge pressure	Γ_0	Γ_0	Γ_1/Γ_0
Pa	s^{-1}	s^{-1}	
6.4	8.7×10^{15}	1.14×10^{15}	0.13
5.0	6.9×10^{15}	5.4×10^{14}	0.12
2.7	3.6×10^{15}	3.4×10^{14}	0.094

Table 7.3 Dissociation efficiency of bottle B

Discharge power is 1 W, collimator is 0.005 mm radius by 1 mm long, Γ_0 is the estimated total flux, and Γ_1 is the atomic flux.

Discharge pressure	Γ_0	Γ_1	Γ_1/Γ_0
Pa	s^{-1}	s^{-1}	
8.0	1.4×10^{15}	3.6×10^{14}	0.26
5.0	6.8×10^{14}	2.3×10^{14}	0.34
3.7	5.1×10^{14}	1.15×10^{14}	0.23

Table 7.4 Dissociation efficiency of bottle C

Discharge power is 1 W, collimator is 0.05 mm by 1 mm long, Γ_0 is the estimated total flux, and Γ_1 is the atomic flux.

Discharge pressure	Γ_0	Γ_1	Γ_1/Γ_0
Pa	s^{-1}	s^{-1}	
14.6	1.65×10^{15}	7.4×10^{14}	0.45
6.9	9.8×10^{14}	3.6×10^{14}	0.37
3.4	4.3×10^{14}	1.75×10^{14}	0.41

12. References

[1] Handbook of Physics, edited by E.U. Condon and H. Odishaw, (second edition, McGraw-Hill 1967.)

[2] J.L. Park, R.E. Voshall, and A.V. Phelps, "Drift Velocities of Slow Electrons in Krypton, Zenon, Deuterium, Carbon Monoxide, Carbon Dioxide, Water Vapor, Nitrous Oxide and Ammonia," Phys. Rev. 127, 2084-2089 (1962).

[3] H.S.W. Massey and E.H.S. Burhop, Electronic and Ionic Impact Phenomena, Clarendon Press, Oxford, England, 1952.

[4] Vroom and de Heer, "Production of Excited Atoms by Impact of Fast Electrons on Molecular Hydrogen and Deuterium," J. Chem. Phys. 50, 580 (1969).

[5] M.J. Mumma and E.C. Zipf, "Dissociative Excitation of Vacuum Emission Features by Electron Impact on Moleculor Gases I, H_2 and O_2," J. Chem. Phys. 55, 1661 (1971).

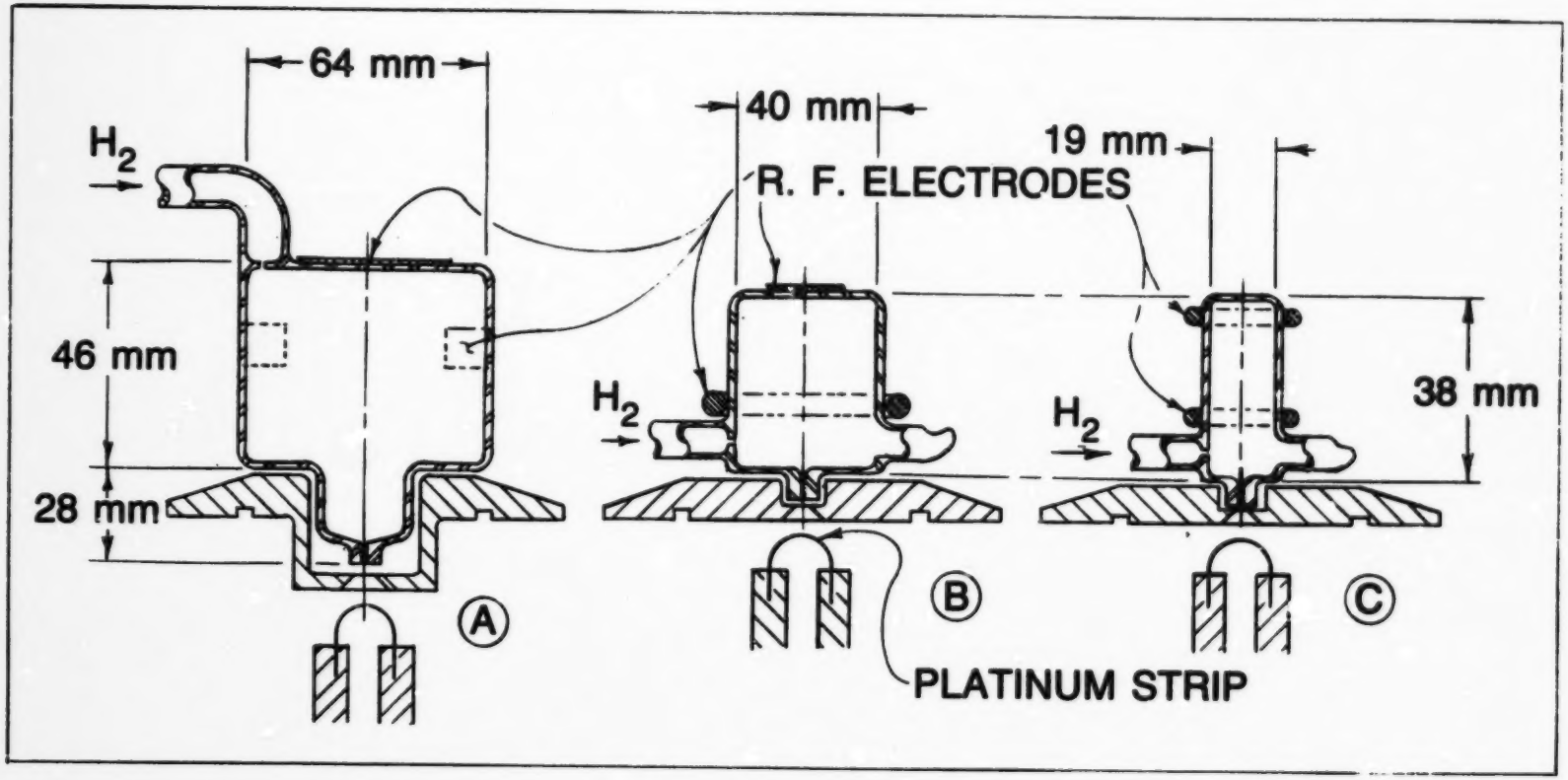

Figure 2.1 The dissociator bottles.

BEST COPY AVAILABLE

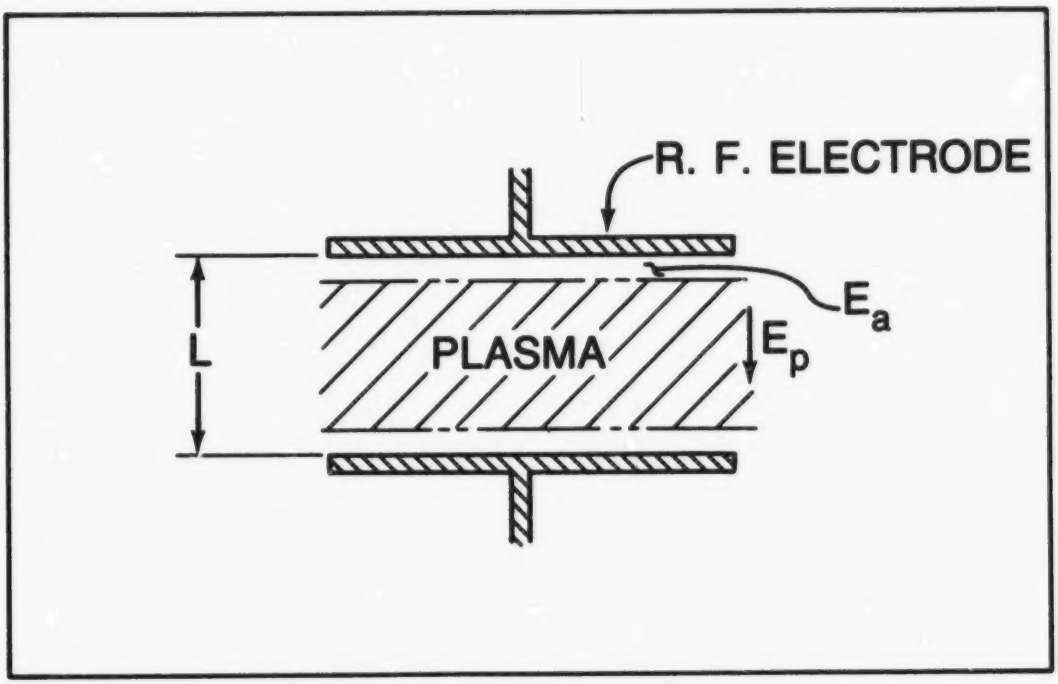

Figure 2.2 The plane-parallel case.

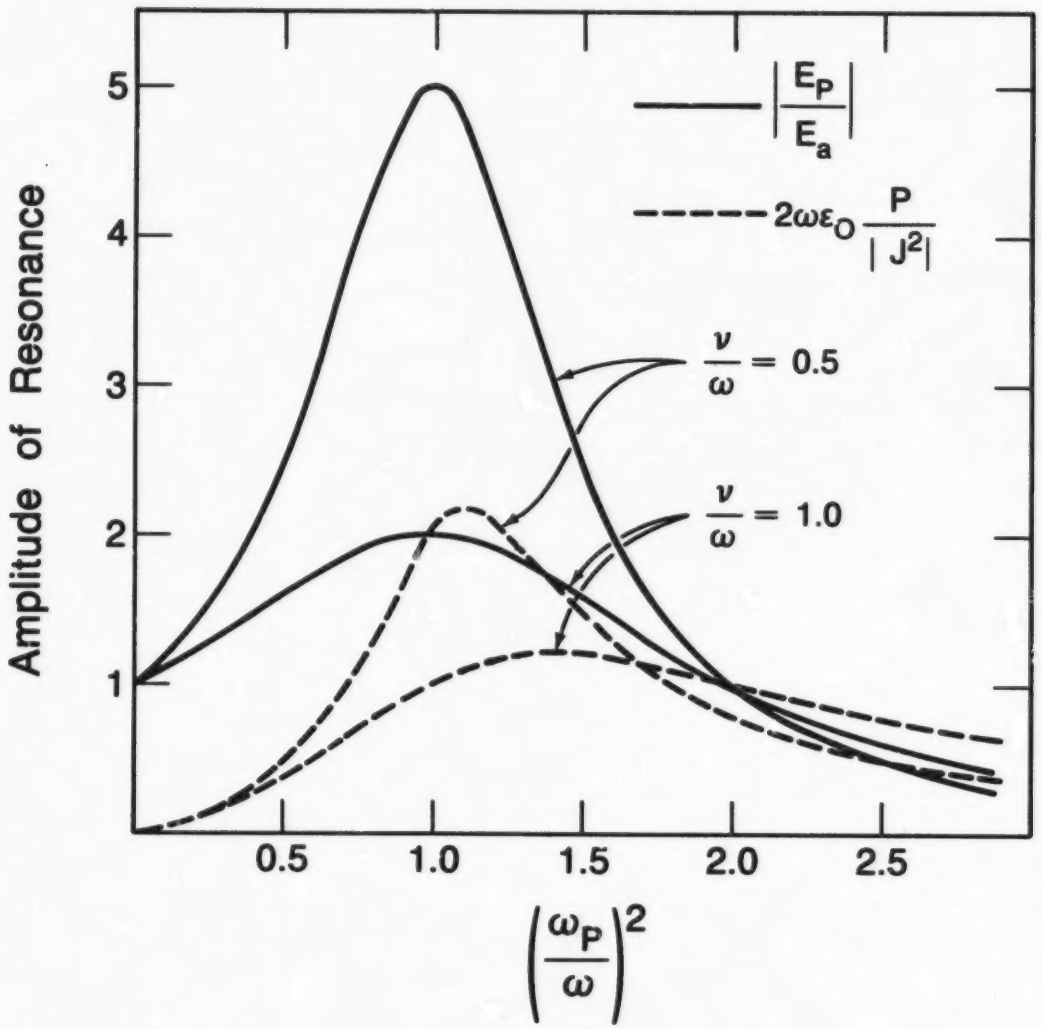

Figure 2.3 The plasma resonance.

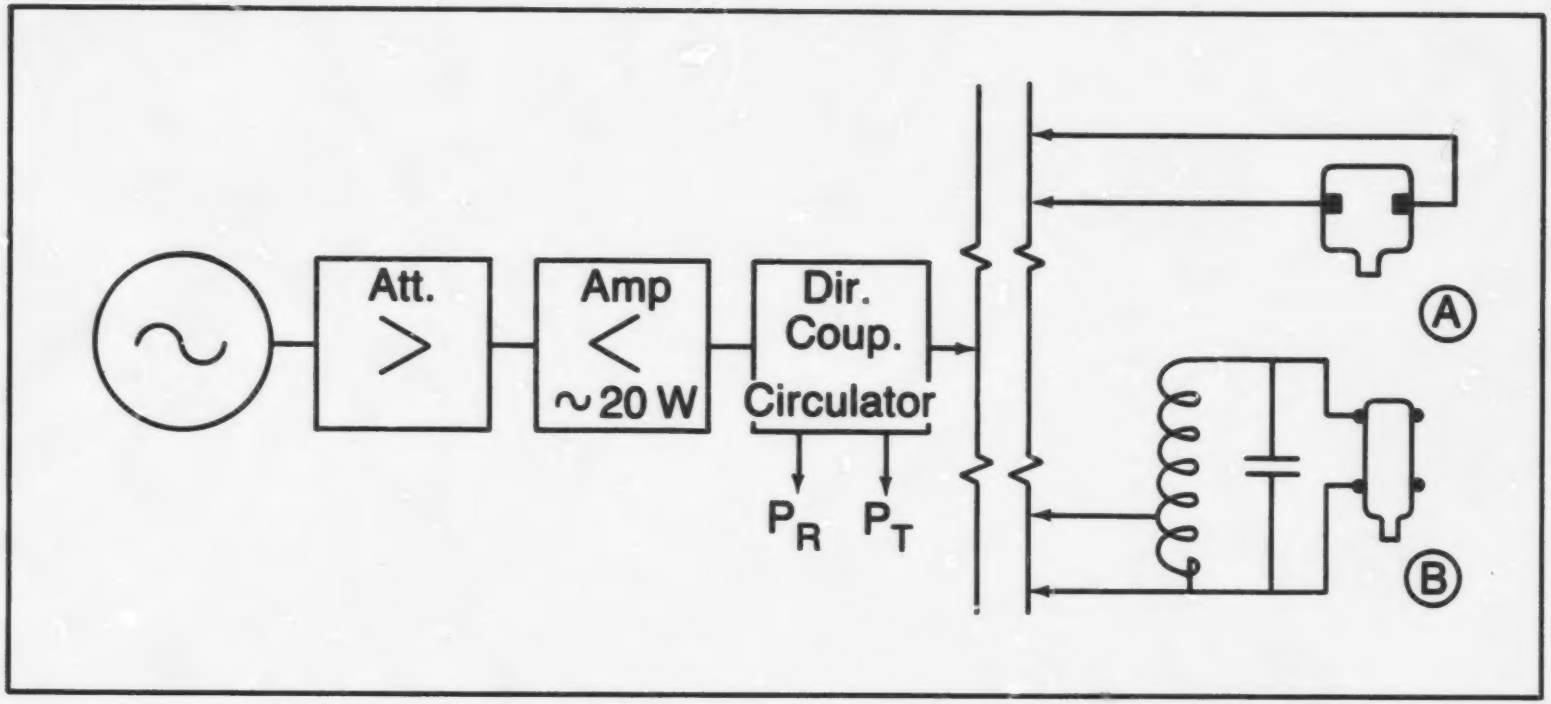

Figure 3.1 The rf circuit.

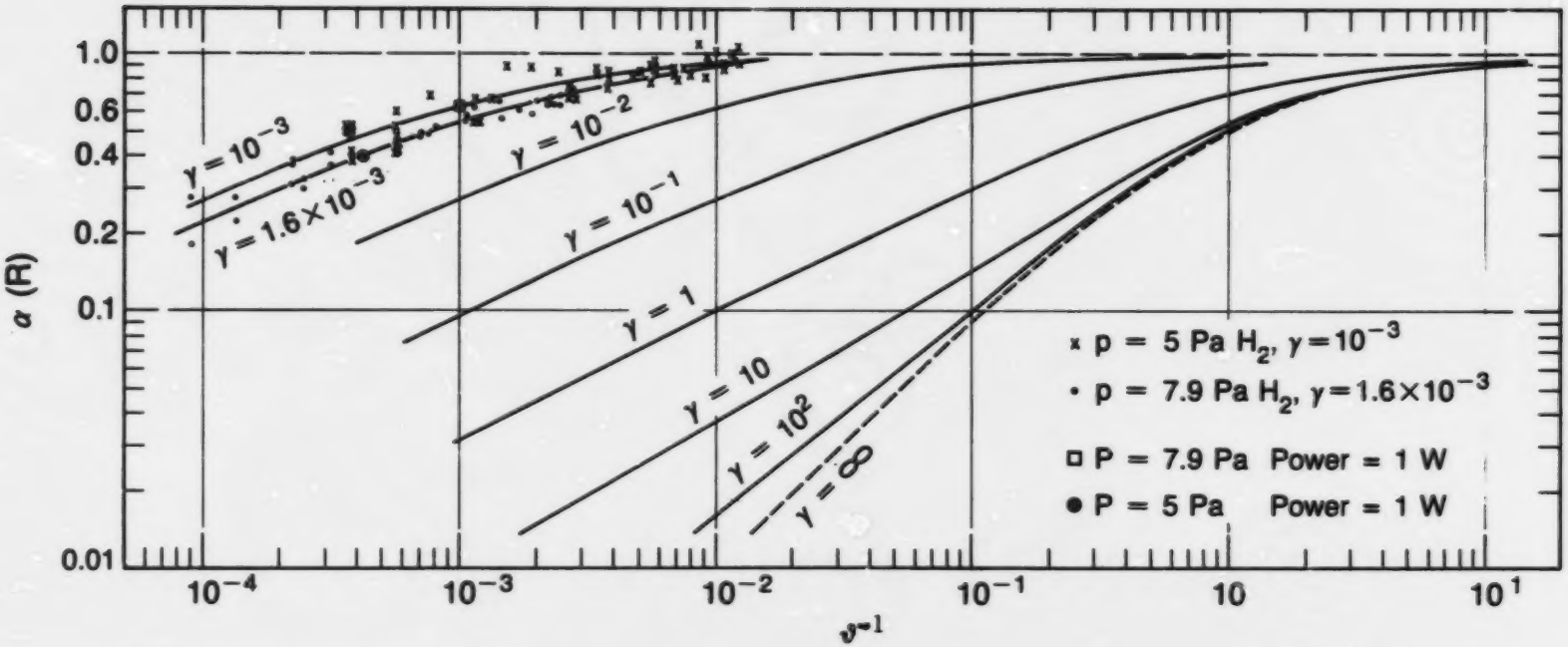

Figure 5.1 The degree of dissociation.

BEST COPY AVAILABLE

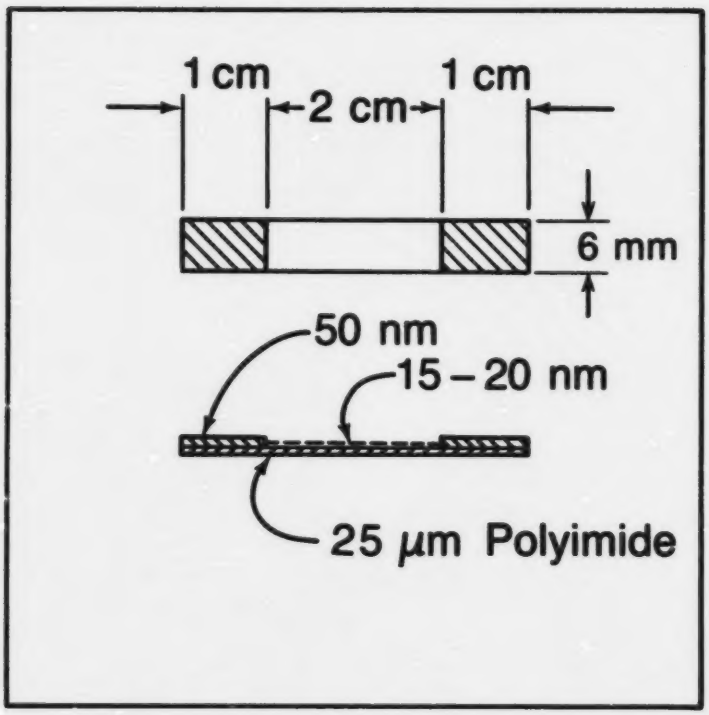

Figure 6.1 The platinum element.

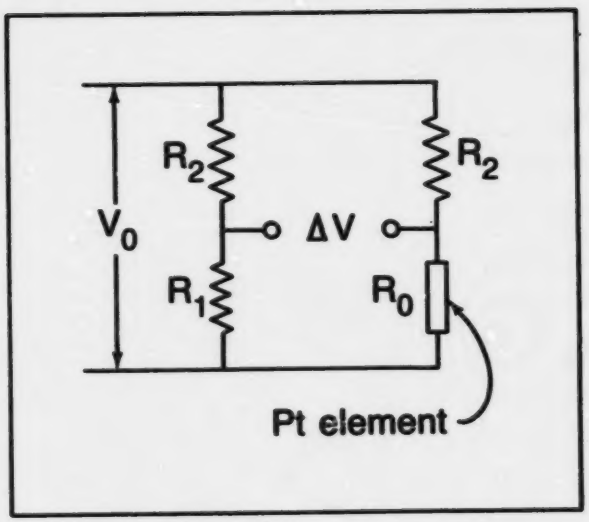

Figure 6.2 The bridge circuit.

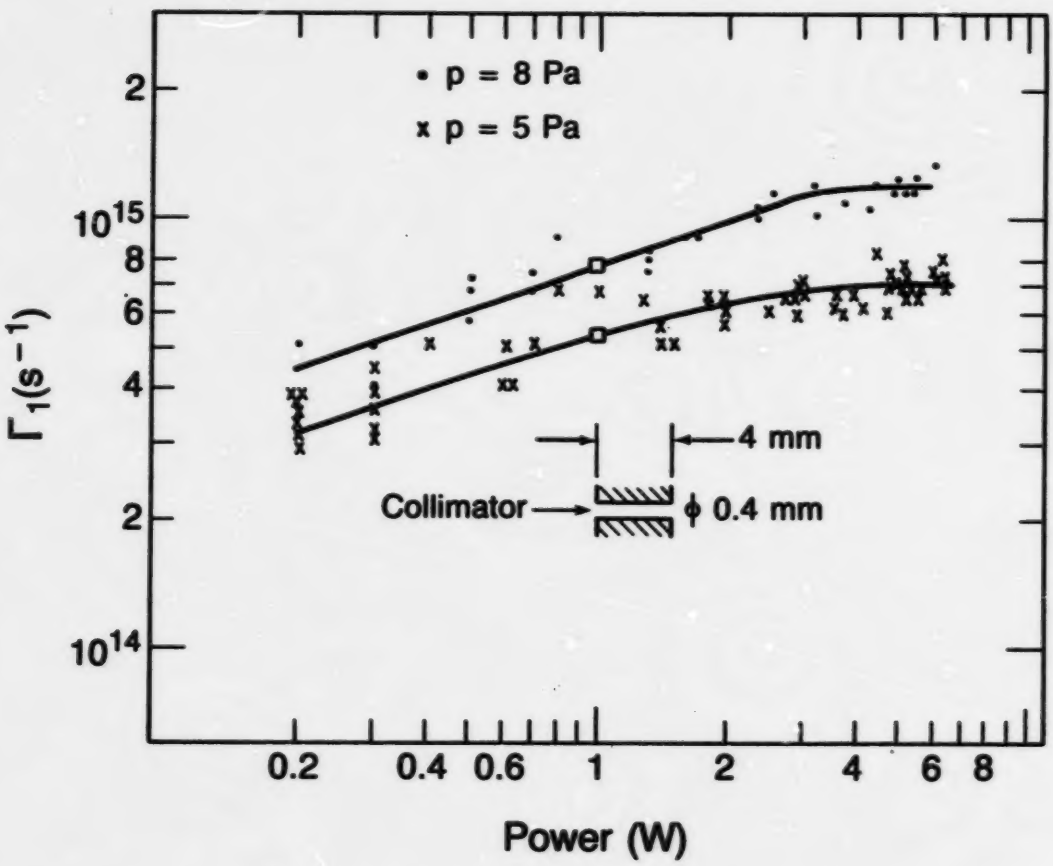

Figure 7.1 Atom flux versus power. Bottle A.

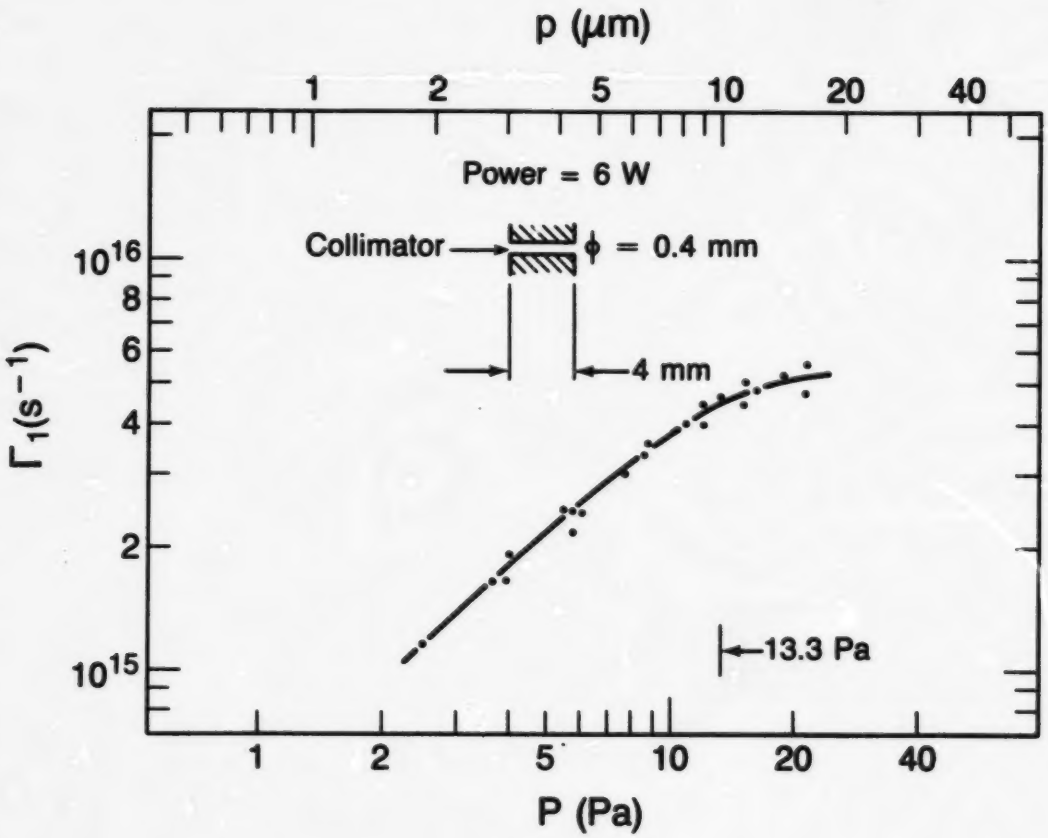

Figure 7.2 Atom flux versus pressure. Bottle B.

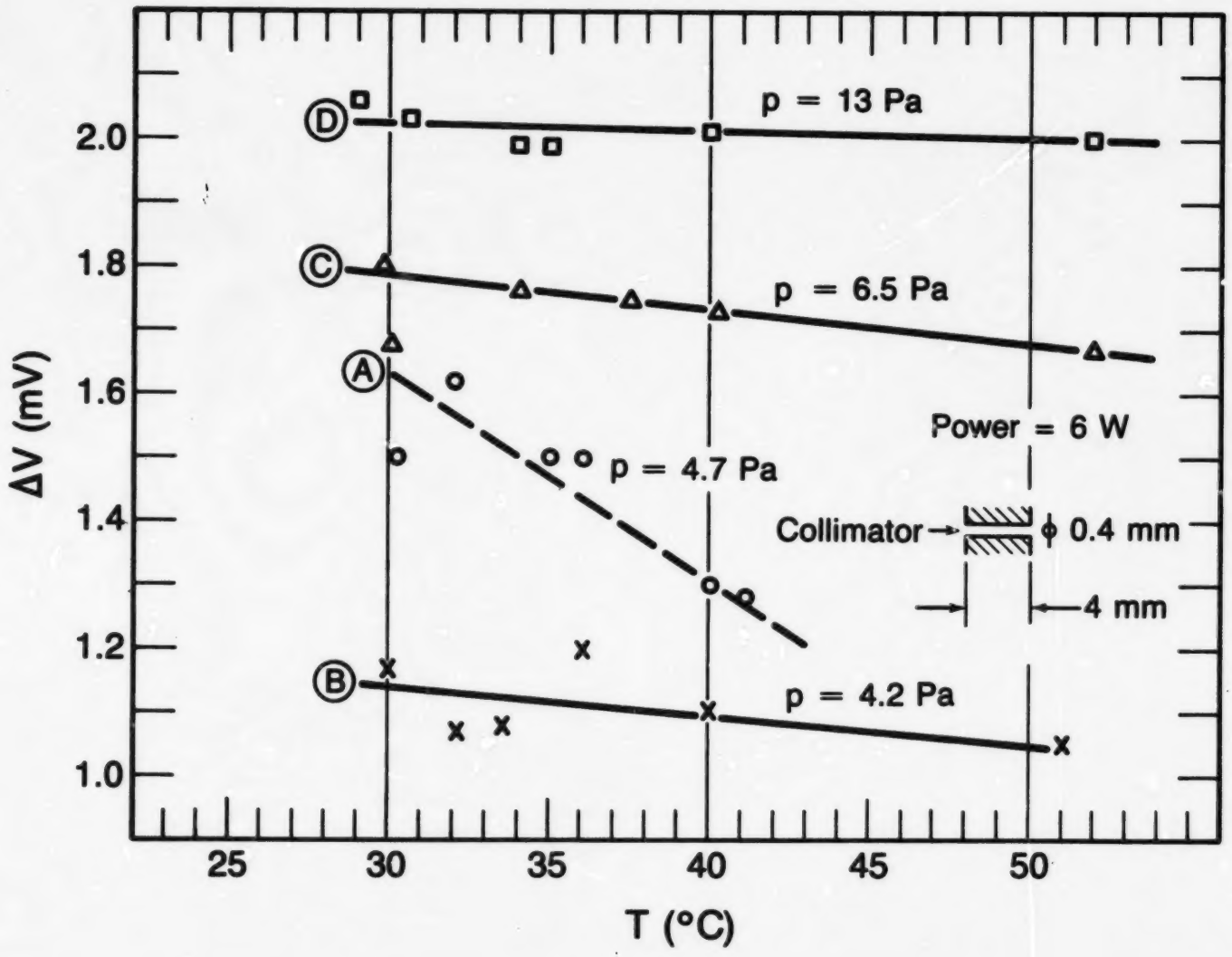

Figure 7.3 Atom flux versus temperature. Bottle A.

43

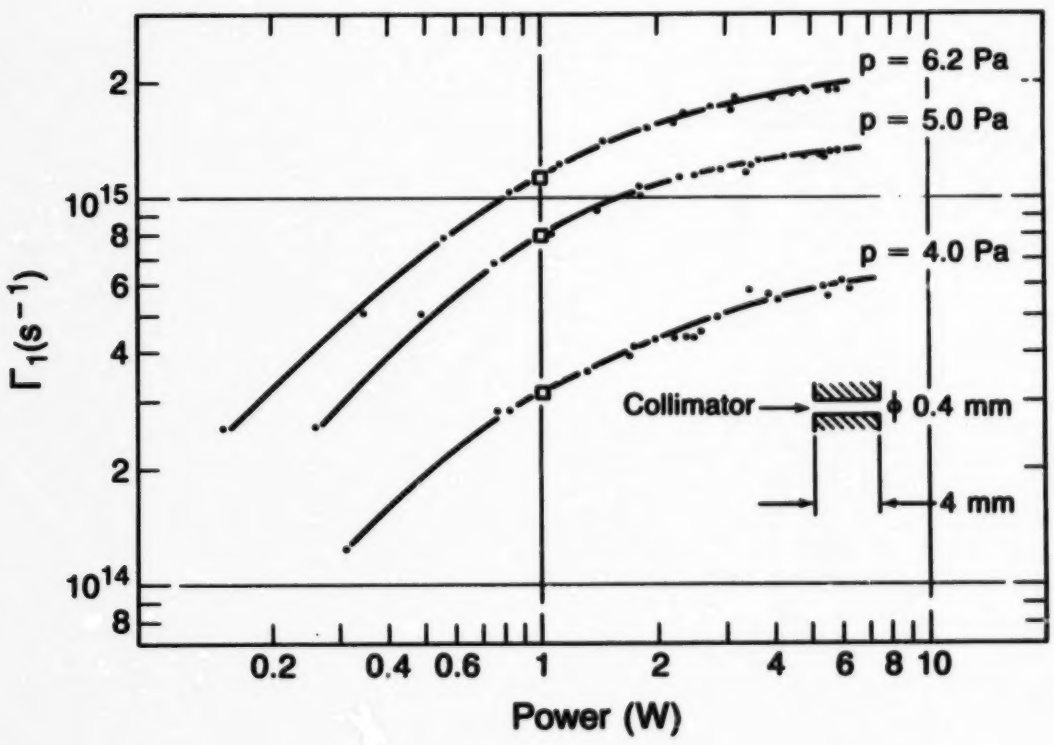

Figure 7.4 Atom flux versus power. Bottle B.

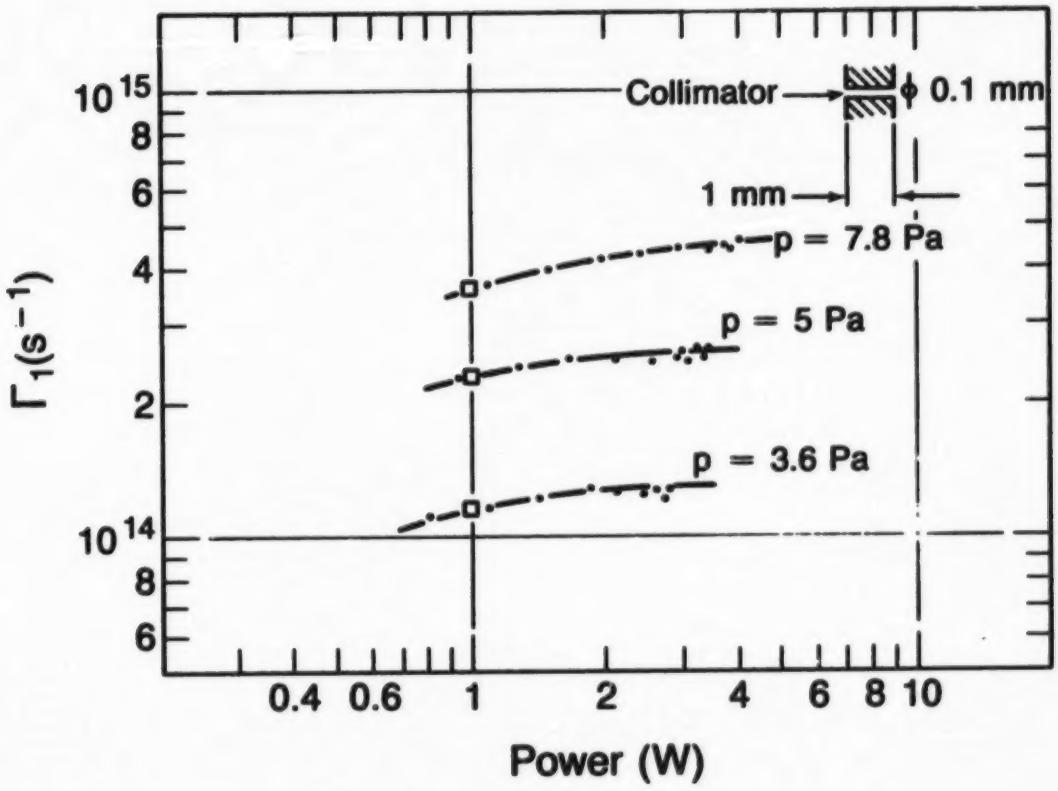

Figure 7.5 Atom flux versus power. Bottle B.

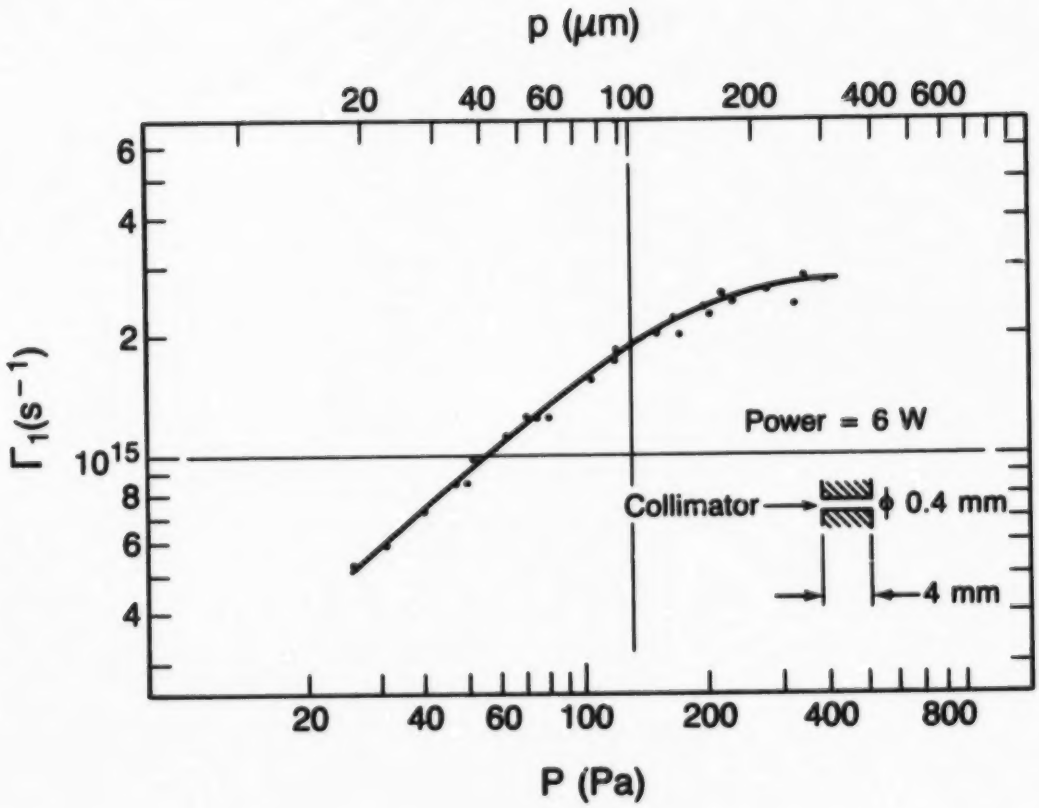

Figure 7.6 Atom flux versus pressure. Bottle B.

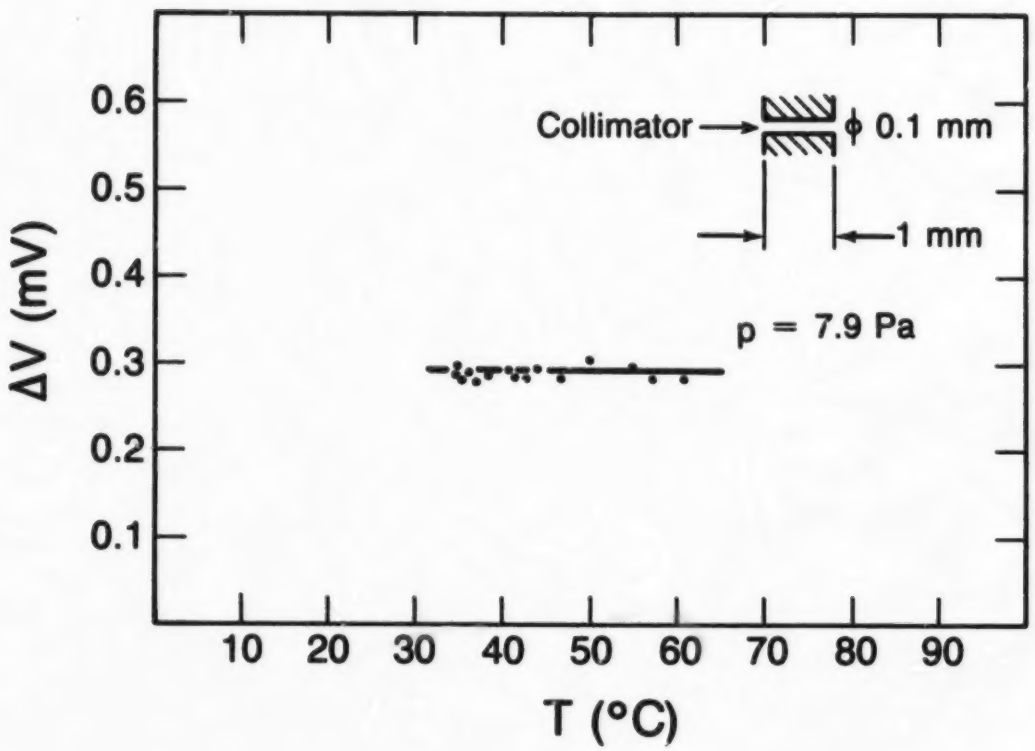

Figure 7.7 Atom flux versus temperature. Bottle B.

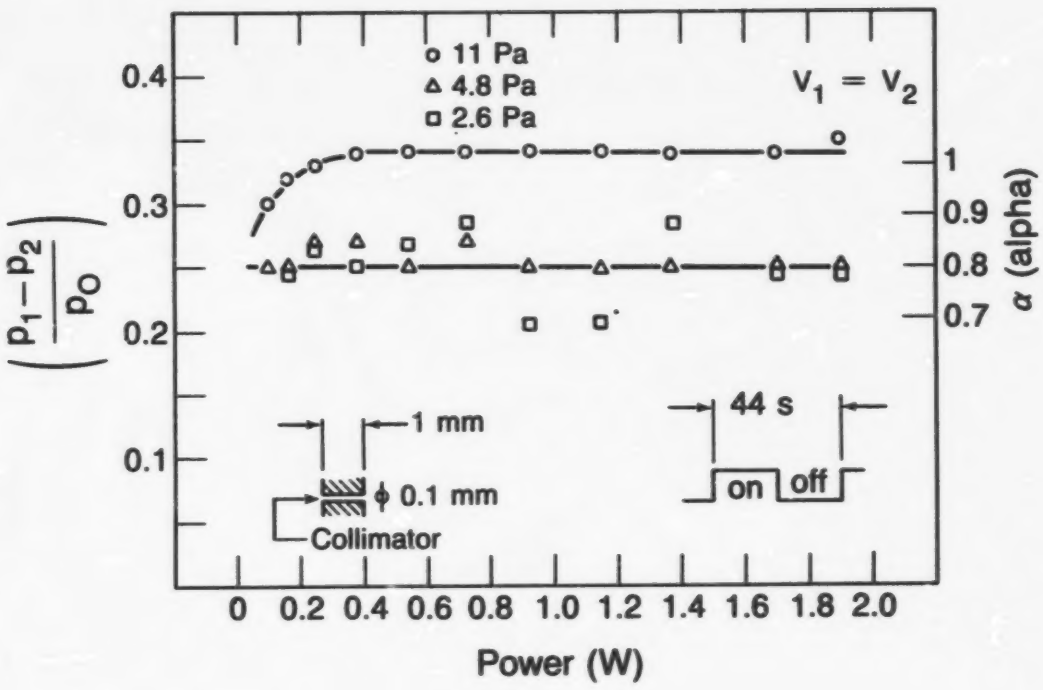

Figure 7.8 Pressure change versus power. Bottle B.

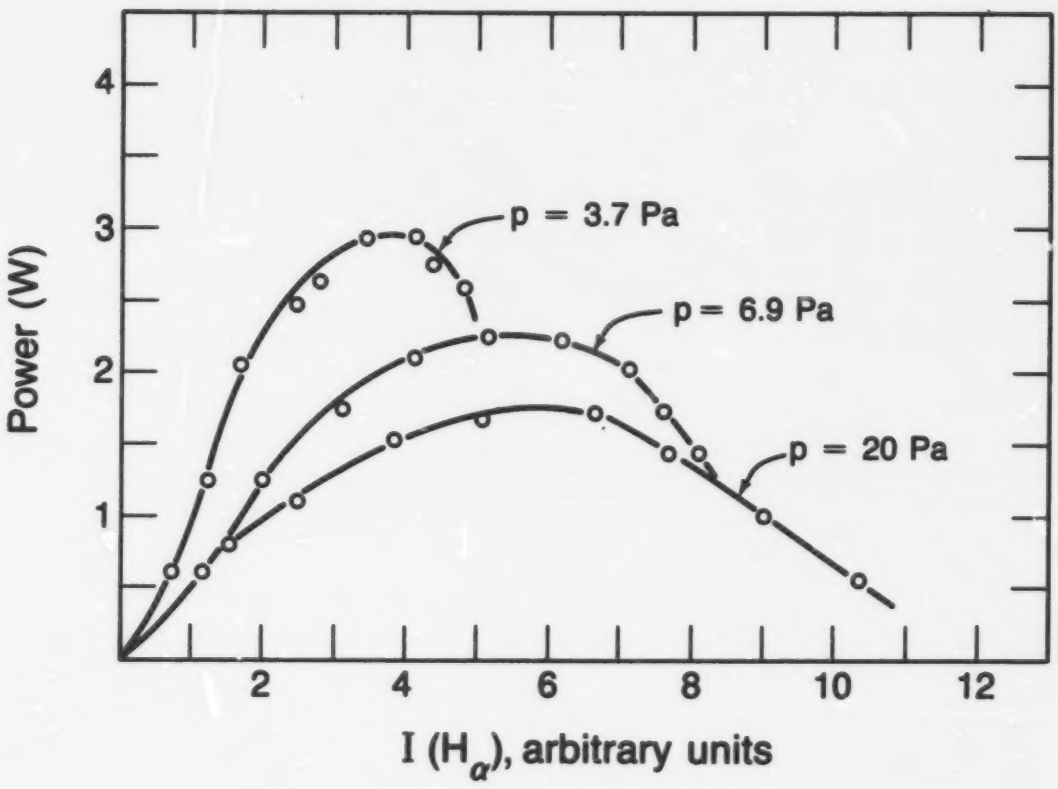

Figure 7.9 Power versus H_α intensity. Bottle C.

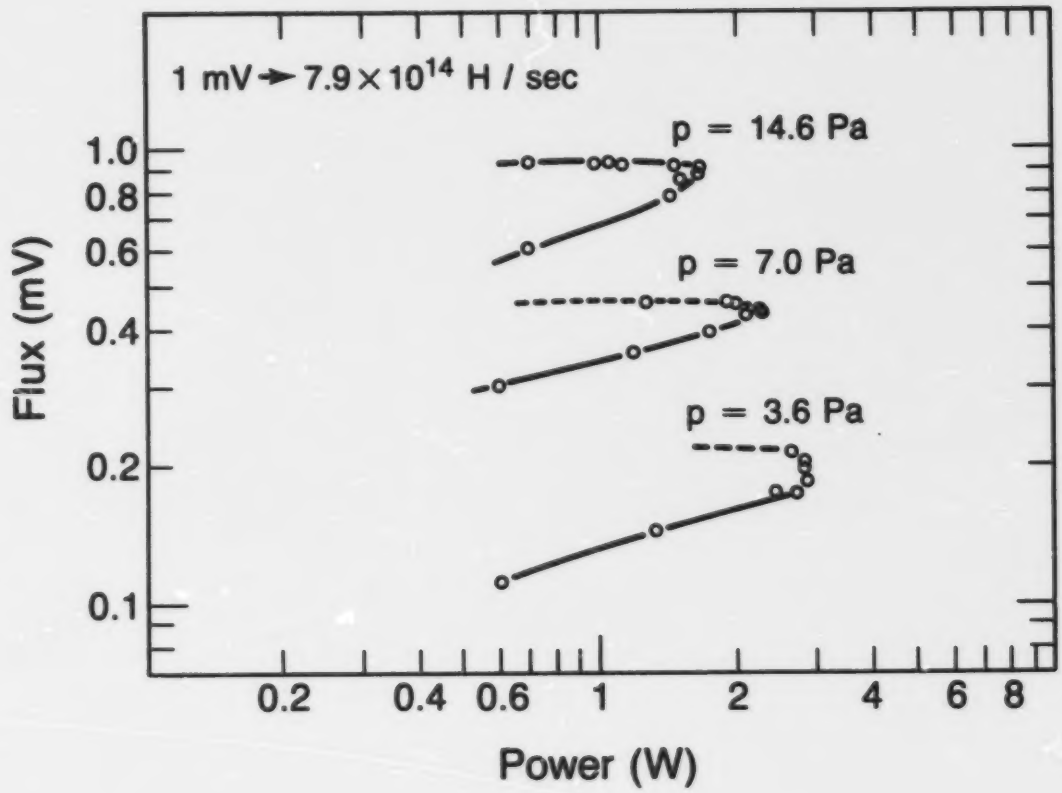

Figure 7.10 Atom flux and plasma resonance.

NBS-114A (REV. 2-8C)

U.S. DEPT. OF COMM. BIBLIOGRAPHIC DATA SHEET (See instructions)	1. PUBLICATION OR REPORT NO. NBS/TN-1315	2. Performing Organ. Report No.	3. Publication Date April 1988

4. TITLE AND SUBTITLE

Investigation of the Hydrogen Source for Masers

5. AUTHOR(S)

K.B. Persson and F.L. Walls

6. PERFORMING ORGANIZATION (If joint or other than NBS, see instructions)

NATIONAL BUREAU OF STANDARDS
DEPARTMENT OF COMMERCE
WASHINGTON, D.C. 20234

7. Contract/Grant No.

8. Type of Report & Period Covered

9. SPONSORING ORGANIZATION NAME AND COMPLETE ADDRESS (Street, City, State, ZIP)

Naval Research Laboratories
Washington, DC 20375

10. SUPPLEMENTARY NOTES

☐ Document describes a computer program; SF-185, FIPS Software Summary, is attached.

11. ABSTRACT (A 200-word or less factual summary of most significant information. If document includes a significant bibliography or literature survey, mention it here)

Various engineering and phenomenological aspects of the radio frequency discharge source for atomic hydrogen used in the masers have been investigated theoretically and experimentally to provide a base for minimizing the size of the source and its power consumption. A scheme and detector have been devised, permitting absolute detection of the atomic beam, and an atom-atom surface recombination theory was developed, applicable to the detector as well as to the walls of the discharge vessel. A self-starting radio frequency circuit, allowing as little as 0.1 W power consumption by the atom source, has been developed.

12. KEY WORDS (Six to twelve entries; alphabetical order; capitalize only proper names; and separate key words by semicolons)

atomic hydrogen; atomic hydrogen detection; dissociation efficiency; hydrogen maser; radio frequency discharge; surface-recombination.

13. AVAILABILITY

☒ Unlimited

☐ For Official Distribution. Do Not Release to NTIS

☒ Order From Superintendent of Documents, U.S. Government Printing Office, Washington, D.C. 20402.

☐ Order From National Technical Information Service (NTIS), Springfield, VA. 22161

14. NO. OF PRINTED PAGES 56

15. Price

U.S. Government Printing Office: 1988—575-378/85142

USCOMM-DC 6043-P80

NBS Technical Publications

Periodical

Journal of Research—The Journal of Research of the National Bureau of Standards reports NBS research and development in those disciplines of the physical and engineering sciences in which the Bureau is active. These include physics, chemistry, engineering, mathematics, and computer sciences. Papers cover a broad range of subjects, with major emphasis on measurement methodology and the basic technology underlying standardization. Also included from time to time are survey articles on topics closely related to the Bureau's technical and scientific programs. Issued six times a year.

Nonperiodicals

Monographs—Major contributions to the technical literature on various subjects related to the Bureau's scientific and technical activities.

Handbooks—Recommended codes of engineering and industrial practice (including safety codes) developed in cooperation with interested industries, professional organizations, and regulatory bodies.

Special Publications—Include proceedings of conferences sponsored by NBS, NBS annual reports, and other special publications appropriate to this grouping such as wall charts, pocket cards, and bibliographies.

Applied Mathematics Series—Mathematical tables, manuals, and studies of special interest to physicists, engineers, chemists, biologists, mathematicians, computer programmers, and others engaged in scientific and technical work.

National Standard Reference Data Series—Provides quantitative data on the physical and chemical properties of materials, compiled from the world's literature and critically evaluated. Developed under a worldwide program coordinated by NBS under the authority of the National Standard Data Act (Public Law 90-396). NOTE: The Journal of Physical and Chemical Reference Data (JPCRD) is published quarterly for NBS by the American Chemical Society (ACS) and the American Institute of Physics (AIP). Subscriptions, reprints, and supplements are available from ACS, 1155 Sixteenth St., NW, Washington, DC 20056.

Building Science Series—Disseminates technical information developed at the Bureau on building materials, components, systems, and whole structures. The series presents research results, test methods, and performance criteria related to the structural and environmental functions and the durability and safety characteristics of building elements and systems.

Technical Notes—Studies or reports which are complete in themselves but restrictive in their treatment of a subject. Analogous to monographs but not so comprehensive in scope or definitive in treatment of the subject area. Often serve as a vehicle for final reports of work performed at NBS under the sponsorship of other government agencies.

Voluntary Product Standards—Developed under procedures published by the Department of Commerce in Part 10, Title 15, of the Code of Federal Regulations. The standards establish nationally recognized requirements for products, and provide all concerned interests with a basis for common understanding of the characteristics of the products. NBS administers this program as a supplement to the activities of the private sector standardizing organizations.

Consumer Information Series—Practical information, based on NBS research and experience, covering areas of interest to the consumer. Easily understandable language and illustrations provide useful background knowledge for shopping in today's technological marketplace.

Order the above NBS publications from: Superintendent of Documents, Government Printing Office, Washington, DC 20402.

Order the following NBS publications—FIPS and NBSIR's—from the National Technical Information Service, Springfield, VA 22161.

Federal Information Processing Standards Publications (FIPS PUB)—Publications in this series collectively constitute the Federal Information Processing Standards Register. The Register serves as the official source of information in the Federal Government regarding standards issued by NBS pursuant to the Federal Property and Administrative Services Act of 1949 as amended, Public Law 89-306 (79 Stat. 1127), and as implemented by Executive Order 11717 (38 FR 12315, dated May 11, 1973) and Part 6 of Title 15 CFR (Code of Federal Regulations).

NBS Interagency Reports (NBSIR)—A special series of interim or final reports on work performed by NBS for outside sponsors (both government and non-government). In general, initial distribution is handled by the sponsor; public distribution is by the National Technical Information Service, Springfield, VA 22161, in paper copy or microfiche form.

U.S. Department of Commerce
National Bureau of Standards
Gaithersburg, MD 20899

Official Business
Penalty for Private Use $300